

Simultaneously detecting spatiotemporal changes with penalized Poisson regression models

Zerui Zhang, Xin Wang, Xin Zhang, Jing Zhang¹

¹*Department of Statistics, Iowa State University, Ames, IA 50011, USA*

²*Program of Bioinformatics and Computational Biology, Iowa State University, Ames, IA 50011, USA*

Abstract

In the realm of large-scale spatiotemporal data, abrupt changes are commonly occurring across both spatial and temporal domains. This study aims to address the concurrent challenges of detecting change points and identifying spatial clusters within spatiotemporal count data. We introduce an innovative method based on the Poisson regression model, employing doubly fused penalization to unveil the underlying spatiotemporal change patterns. To efficiently estimate the model, we present an iterative shrinkage and threshold based algorithm to minimize the doubly penalized likelihood function. We establish the statistical consistency properties of the proposed estimator, confirming its reliability and accuracy. Furthermore, we conduct extensive numerical experiments to validate our theoretical findings, thereby highlighting the superior performance of our method when compared to existing competitive approaches.

keywords: Change points detection; Fused penalty; Minimum spanning tree; Poisson regression model; Spatial clustering; Spatiotemporal data.

1 Introduction

In disease and epidemiology studies, datasets are commonly represented in the format of spatiotemporal count data ([Schmid and Held, 2004](#); [Tzala and Best, 2008](#)).

This data format encapsulates the total number of identified cases within contiguous non-overlapping areal units over consecutive time periods, offering a comprehensive perspective on the spatial and temporal dynamics of disease prevalence (Ansari et al., 2020). One salient characteristic in the spatiotemporal count data is that observations from geographically proximate areal units and temporally close periods tend to exhibit more similar values than those farther apart (Hardisty and Klippel, 2010). The explicit identification and quantification of fluctuating and changing patterns over both spatial and temporal domains emerge as critical research objectives. This is particularly essential in disease management, where timely insights derived from data mining facilitate the swift implementation of prevention and control measures (Kulldorff, 2001; Kulldorff et al., 2005). Beyond public health and epidemiology, the implications of spatiotemporal count data change detection reverberate across diverse domains, including agriculture (Besag and Higdon, 1999; Paradinas et al., 2017; Zhang and Wang, 2023), environment (Gusev, 2008; Lee et al., 2021), and social science (Law et al., 2014).

Within spatiotemporal count data, the exploration of changes reveals two prominent dimensions: alterations in spatial relationships and shifts in the temporal domain. First, for spatial relationships, clustering has been widely studied and applied, and Ansari et al. (2020) gave a comprehensive review of spatiotemporal clustering approaches. Anderson et al. (2017) employed a Poisson regression model to identify spatial clusters in the yearly counts of respiratory admissions to hospitals. Napier et al. (2019) proposed a new Bayesian approach to identify groups of areal units with similar temporal disease trends. Siljander et al. (2022) used a Poisson space-time scan statistic to detect clusters varied over both time and space in Helsinki. Kulldorff (2001) introduced a space-time scan statistic based on Poisson likelihood, which was applied in different studies (Rogerson, 2001; Güemes et al., 2021; Mohammadi et al., 2022). Assunção et al. (2007) proposed a scored based space-time scan for point processes data. Frévent et al. (2021) and Smida et al. (2022) proposed distribution-free scan statistics for detecting spatial clusters in functional data. Kamenetsky et al. (2022) used a regularized approach to detect spatial clusters, considering time effects through a Poisson regression model. Furthermore, there are methods taking into consideration the effects of covariates in the context of spatiotemporal count data. Jung (2009) constructed a scan statistic based on generalized linear models to adjust the effects of covariates for spatial data. Lee et al. (2017) and Lee et al. (2020) considered spatial cluster detection for regression coefficients based on hypothesis tests. Lee et al. (2021) extended the approach to spatiotemporal data based on a varying coefficient regression model. In recent studies, the penalization method has been adopted to discover model-based clusters through regression coefficients in

spatial data (Li and Sang, 2019; Wang, 2023; Ma et al., 2020; Wang et al., 2023b; Lin et al., 2022). Specifically, these approaches incorporate the fusion penalty to have sparsity in the differences of model coefficients. A zero coefficient difference implies that two locations will have the same estimated coefficients, which indicates that they come from the same cluster.

When delving into the changes over the time domain, temporal changes are often studied separately from spatial clustering through change point detection. For example, the CUSUM procedure (or cumulative summation) is a well-known method for temporal change-point detection (Cho and Fryzlewicz, 2015; Cho, 2016; Gromenko et al., 2017; Wang and Samworth, 2018). The CUSUM transformation generates test statistics, which will be compared with the standard Brownian Bridge to test the existence of the change point. However, the traditional CUSUM method cannot be easily applied to detect temporal change points over large-scale spatial domains. Altieri et al. (2015) introduced the Bayesian approach by log-Gaussian Cox process model, and the posterior distribution of the potential change-point distribution assumed the spatial homogeneous setup. Score statistics that capture changes in the mean and/or the spatiotemporal covariance were discussed under the spatiotemporal data in Xie and Siegmund (2012). Harchaoui and Lévy-Leduc (2010) used fused lasso to detect multiple change points in time series data and was extended to autoregressive time series models (Chan et al., 2014) and least absolute deviation based models (Li and Wang, 2020). Note that none of the temporal change-point detection methods mentioned above can handle the covariate effects.

However, to the best of our knowledge, there is currently no penalization method in the literature aforementioned that can simultaneously address the tasks of change points detection and spatial clusters identification with the consideration of covariates. In this work, we propose a novel penalized approach to simultaneously address the tasks of detecting change points and identifying spatial clusters for count data. We formulate an optimization problem based on Poisson likelihood and two penalty terms: a fused penalty for detecting change points and an adaptive spanning tree based fusion penalty for identifying spatial clusters. We develop an algorithm to solve the doubly-penalized estimation problem. We also investigate the theoretical properties of our proposed estimator. It is shown that our estimator is statistically consistent and has the capability to reveal spatial clusters and temporal changes with probability one. Our theoretical findings are also validated by thorough numerical experiments. Besides, covariates are also incorporated in the modeling to ensure that the detected spatial and temporal changes are robust and appropriately adjusted for relevant covariate influences.

The article is organized as follows. In Section 2, we will propose our model and

develop the model estimation method. In Section 3, we will establish the theoretical properties of our proposed estimator. In Section 4, we will conduct simulation studies to evaluate our proposed approach under different scenarios. The proposed approach will be applied to a real example in Section 5.

2 Methodology

In Section 2.1, we introduce the statistical model and the optimization problem. And in Section 2.2, we present the proposed algorithm to solve the optimization problem.

2.1 Statistical Model

Let y_{it} be the observed count and n_{it} be the population size for location i at time t , where $i = 1, \dots, N$ and $t = 1, \dots, T$. Consider the following Poisson regression model,

$$y_{it} \sim \text{Poisson}(n_{it}\mu_{it}), \quad (1)$$

where μ_{it} is the rate with $E(y_{it}) = n_{it}\mu_{it}$. If y_{it} denotes the number of deaths for a specific cancer, then μ_{it} represents the mortality rate. We will model μ_{it} based on covariates effects and time effects. Generally, we assume two types of covariates, as in Ma et al. (2020) and Wang et al. (2023b). Specifically, \mathbf{z}_{it} is the covariate vector with dimension q , which has common effects across all locations, and \mathbf{x}_{it} is the covariate vector with dimension p , which has location-specific effects. Assume the following model for μ_{it} ,

$$\log \mu_{it} = \mathbf{z}_{it}^\top \boldsymbol{\alpha} + \mathbf{x}_{it}^\top \boldsymbol{\beta}_i + \eta_t, \quad (2)$$

where $\boldsymbol{\alpha}$ represents the vector of common regression coefficients shared by global effects, $\boldsymbol{\beta}_i$'s are location-specific regression coefficients, and η_t is the time effect. A special case is that $\mathbf{x}_{it} = 1$, which represents the location-specific intercept. Then, the model will have a simplified form,

$$\log \mu_{it} = \mathbf{z}_{it}^\top \boldsymbol{\alpha} + \beta_i + \eta_t. \quad (3)$$

Assume that N locations are from K underlying spatial clusters $\{\mathcal{C}_k\}_{k=1}^K$, where \mathcal{C}_k contains the locations belonging to cluster k . That is $\boldsymbol{\beta}_i = \boldsymbol{\beta}_{i'}$ if location i and location i' are both in cluster k , for $k = 1, \dots, K$. Furthermore, assume that there are J change points t_j^* such that $\eta_t = \tau_j$ if $t_{j-1}^* \leq t \leq t_j^* - 1$ for $j = 1, \dots, J + 1$

with $t_0^* = 1$ and $t_{j+1}^* = T + 1$. For an identifiability purpose, we assume that $\eta_1 = 0$, indicating that $\tau_1 = 0$. Our goal is to use observed data to estimate the number of clusters \hat{K} , the corresponding cluster structure $\hat{\mathcal{C}} = \{\hat{\mathcal{C}}_1, \dots, \hat{\mathcal{C}}_{\hat{K}}\}$, the estimated regression coefficients $\hat{\boldsymbol{\alpha}}, \hat{\boldsymbol{\beta}}_i$, the number of changed points \hat{J} , and the corresponding time effects $\hat{\eta}_t$.

To achieve the goal, we will construct an optimization problem based on the following likelihood function and two sets of penalty functions. Let $\boldsymbol{\eta} = (\eta_1, \eta_2, \dots, \eta_T)^\top$ and $\boldsymbol{\beta} = (\boldsymbol{\beta}_1^\top, \dots, \boldsymbol{\beta}_N^\top)^\top$, the negative loglikelihood function based on the model in (1) and (2) is

$$l_0(\boldsymbol{\alpha}, \boldsymbol{\eta}, \boldsymbol{\beta}) = \sum_{i=1}^N \sum_{t=1}^T \left[-y_{it} \left(\log n_{it} + \mathbf{z}_{it}^\top \boldsymbol{\alpha} + \mathbf{x}_{it}^\top \boldsymbol{\beta}_i + \eta_t \right) + n_{it} \exp \left(\mathbf{z}_{it}^\top \boldsymbol{\alpha} + \mathbf{x}_{it}^\top \boldsymbol{\beta}_i + \eta_t \right) \right]. \quad (4)$$

To find change points, we consider a fused type penalty on time effects as proposed in [Harchaoui and Lévy-Leduc \(2010\)](#), which has the following form,

$$\sum_{t=2}^T \mathcal{P}_{\gamma_1} (|\eta_t - \eta_{t-1}|, \lambda_1), \quad (5)$$

where $\mathcal{P}_{\gamma_1}(\cdot; \lambda_1)$ is the minimax concave penalty (MCP) ([Zhang, 2010](#)) with the following form

$$\mathcal{P}_{\gamma}(t; \lambda) = \begin{cases} \lambda|t| - \frac{t^2}{2\gamma}, & |t| \leq \gamma\lambda, \\ \frac{1}{2}\gamma\lambda^2, & |t| > \gamma\lambda. \end{cases} \quad (6)$$

γ is a built-in parameter, which is fixed at 3 as in the literature ([Ma et al., 2020](#)), λ is a tuning parameter, which will be selected based data driven criteria. If $|\eta_t - \eta_{t-1}|$ is shrunk to zero, no change point is identified at time t . If $|\eta_t - \eta_{t-1}|$ is not shrunk to zero, then a change point at time t is detected. Let $\boldsymbol{\xi} = (\xi_2, \dots, \xi_T)^\top = (\eta_2 - \eta_1, \eta_3 - \eta_2, \dots, \eta_T - \eta_{T-1})^\top$, then, $(\eta_2, \dots, \eta_T)^\top = \mathbf{M}\boldsymbol{\xi}$, where \mathbf{M} is a $(T-1) \times (T-1)$ lower triangular matrix with nonzero elements equal to one. Thus (5) can be written as,

$$\sum_{t=2}^T \mathcal{P}_{\gamma_1} (|\eta_t - \eta_{t-1}|, \lambda_1) = \sum_{t=2}^T \mathcal{P}_{\gamma_1} (|\xi_t|, \lambda_1). \quad (7)$$

(7) implies that detecting zero differences between η_t and η_{t-1} is equivalent to detecting zero values of ξ_t .

To find the spatial cluster pattern, we will consider a graph based fusion penalty. Let \mathcal{G} be an undirected connected graph $\mathcal{G} = (\mathcal{V}, \mathcal{E}_0)$, where $\mathcal{V} = \{v_1, \dots, v_N\}$ is the

set of vertices with v_i representing location i , and $\mathcal{E}_0 = \{(v_i, v_{i'}) : v_i \neq v_{i'}\}$ is the edge set. In areal data, we can construct this graph based on neighbor structure: if area i and area i' share a boundary, then $(v_i, v_{i'}) \in \mathcal{E}_0$. In geostatistical data, we can construct this graph based on Delaunay triangulation (Lee and Schachter, 1980). A spanning tree \mathcal{T} of the graph \mathcal{G} is a connected undirected subgraph of \mathcal{G} with no cycles and includes all the vertices of \mathcal{G} . A special spanning tree is a minimum spanning tree (MST). Denote $d(v_i, v_{i'})$ as the associated weight to each edge $(v_i, v_{i'})$ in \mathcal{E}_0 , then a MST is defined as $\mathcal{T} = (\mathcal{V}, \mathcal{E})$ such that this subgraph is a spanning tree and $\sum_{(v_i, v_{i'}) \in \mathcal{E}} d(v_i, v_{i'})$ is minimized (Li and Sang, 2019). The construction of MST relies on the edge weights for all edges in \mathcal{E} . If there is some prior knowledge of the weights, the weights can be constructed based on local estimates as used in Zhang et al. (2022); Wang et al. (2023a). If there are no local estimates, one can use distance to define weights for geographical data as used in Li and Sang (2019). If the weights are not properly defined, MST will be constructed based on equal weights. The tree based penalty for a given an MST, \mathcal{T} , is defined as

$$\sum_{(i, i') \in \mathcal{E}} \mathcal{P}_{\gamma_2} (\|\beta_i - \beta_{i'}\|, \lambda_2), \quad (8)$$

where $\mathcal{P}_{\gamma_2}(\cdot; \lambda_2)$ is the MCP with $\gamma_2 = 3$ and λ_2 is a tuning parameter that will be selected later.

Based on the property of MST, we can establish an incident matrix \mathbf{H} for \mathcal{T} , which is an $(N - 1) \times N$ full rank matrix. And the (l, i) th entry in \mathbf{H} is defined as:

$$\mathbf{H}_{l,i} = \begin{cases} 1, & \text{if } i = s(l), \\ -1, & \text{if } i = e(l), \text{ where } s(l) \text{ and } e(l) \text{ denote the starting and ending node} \\ 0, & \text{otherwise,} \end{cases}$$

indices of edge l in \mathcal{T} , respectively, with $s(l) < e(l)$. Then, $(\beta_i^\top - \beta_{i'}^\top, (i, i') \in \mathcal{T}) = (\mathbf{H} \otimes \mathbf{I}_p) \beta$. Let $\tilde{\mathbf{H}} = \begin{pmatrix} \frac{1}{\sqrt{N}} \mathbf{1}^\top \\ \mathbf{H} \end{pmatrix}$, which is an $N \times N$ full rank matrix. Then, we can define $\boldsymbol{\varsigma} = (\boldsymbol{\varsigma}_1^\top, \boldsymbol{\varsigma}_2^\top, \dots, \boldsymbol{\varsigma}_N^\top)^\top = (\tilde{\mathbf{H}} \otimes \mathbf{I}_p) \beta$. And $\beta = (\tilde{\mathbf{H}} \otimes \mathbf{I}_p)^{-1} \boldsymbol{\varsigma} = (\tilde{\mathbf{H}}^{-1} \otimes \mathbf{I}_p) \boldsymbol{\varsigma}$. Thus, (8) can be written as

$$\sum_{(i, i') \in \mathcal{E}} \mathcal{P}_{\gamma_2} (\|\beta_i - \beta_{i'}\|, \lambda_2) = \sum_{i=2}^N \mathcal{P}_{\gamma_2} (\|\boldsymbol{\varsigma}_i\|, \lambda_2). \quad (9)$$

And (9) implies that detecting zero differences between β_i and $\beta_{i'}$ is equivalent to detecting zero values of $\boldsymbol{\varsigma}_i$.

To achieve the goal of identifying change points and finding cluster patterns simultaneously, we consider minimizing the following objective function, which combines

the likelihood function in (4), the penalty functions for identifying change points in (5) and the penalty functions for finding clusters in (8),

$$L(\boldsymbol{\alpha}, \boldsymbol{\eta}, \boldsymbol{\beta}) = \frac{1}{NT} \sum_{i=1}^N \sum_{t=1}^T \left[-y_{it} \left(\mathbf{z}_{it}^\top \boldsymbol{\alpha} + \mathbf{x}_{it}^\top \boldsymbol{\beta}_i + \eta_t \right) + n_{it} \exp \left(\mathbf{z}_{it}^\top \boldsymbol{\alpha} + \mathbf{x}_{it}^\top \boldsymbol{\beta}_i + \eta_t \right) \right] \\ + \sum_{t=2}^T \mathcal{P}_{\gamma_1} (|\eta_t - \eta_{t-1}|, \lambda_1) + \sum_{(i,i') \in \mathcal{E}} \mathcal{P}_{\gamma_2} (\|\boldsymbol{\beta}_i - \boldsymbol{\beta}_{i'}\|, \lambda_2). \quad (10)$$

Let $\boldsymbol{\theta} = (\boldsymbol{\alpha}^\top, \boldsymbol{\xi}^\top, \boldsymbol{\varsigma}^\top)^\top$, which is a $(q + T - 1 + Np) \times 1$ vector. Based on (7) and (9), the objective function (10) can be expressed in terms of $\boldsymbol{\theta}$ as follows:

$$Q(\boldsymbol{\theta}) = \frac{1}{NT} \sum_{i=1}^N \sum_{t=1}^T \left[-y_{it} \left(\mathbf{z}_{it}^\top \boldsymbol{\alpha} + \mathbf{x}_{it}^\top \mathbf{h}_i \boldsymbol{\varsigma} + \mathbf{m}_t^\top \boldsymbol{\xi} \right) + n_{it} \exp \left(\mathbf{z}_{it}^\top \boldsymbol{\alpha} + \mathbf{x}_{it}^\top \mathbf{h}_i \boldsymbol{\varsigma} + \mathbf{m}_t^\top \boldsymbol{\xi} \right) \right] \\ + \sum_{t=2}^T \mathcal{P}_{\gamma_1} (|\xi_t|, \lambda_1) + \sum_{i=2}^N \mathcal{P}_{\gamma_2} (\|\boldsymbol{\varsigma}_i\|, \lambda_2), \quad (11)$$

where \mathbf{m}_t^\top is the $(t-1)$ th row of \mathbf{M} for $t = 2, \dots, T$, $\mathbf{m}_1 = \mathbf{0}_{T-1}$, a $(T-1) \times 1$ zero vector, and $\mathbf{h}_i = \tilde{\mathbf{h}}_i^\top \otimes \mathbf{I}_p$ with $\tilde{\mathbf{h}}_i^\top$ is the i th row of $\tilde{\mathbf{H}}^{-1}$.

2.2 Computation algorithm

Let $\hat{\boldsymbol{\theta}} = (\hat{\boldsymbol{\alpha}}^\top, \hat{\boldsymbol{\xi}}^\top, \hat{\boldsymbol{\varsigma}}^\top)^\top$ be the solution to the following minimization problem for a given tree \mathcal{T} and given λ_1 and λ_2 based on the objective function in (11),

$$\hat{\boldsymbol{\theta}} = \arg \min_{\boldsymbol{\theta}} Q(\boldsymbol{\theta}; \lambda_1, \lambda_2). \quad (12)$$

To solve the minimization problem, we develop an algorithm based on the general iterative shrinkage and thresholding algorithm (GIST) (Gong et al., 2013). The details are outlined below.

Denote $l(\boldsymbol{\theta}) = \frac{1}{NT} \sum_{i=1}^N \sum_{t=1}^T \left[-y_{it} \left(\mathbf{z}_{it}^\top \boldsymbol{\alpha} + \mathbf{x}_{it}^\top \mathbf{h}_i \boldsymbol{\varsigma} + \mathbf{m}_t^\top \boldsymbol{\xi} \right) + n_{it} \exp \left(\mathbf{z}_{it}^\top \boldsymbol{\alpha} + \mathbf{x}_{it}^\top \mathbf{h}_i \boldsymbol{\varsigma} + \mathbf{m}_t^\top \boldsymbol{\xi} \right) \right]$. Given the current values of parameters $\boldsymbol{\theta}^{(r)}$ at the r th step, then the $(r+1)$ th update $\boldsymbol{\theta}^{(r+1)}$ is given by,

$$\boldsymbol{\theta}^{(r+1)} = \arg \min_{\boldsymbol{\theta}} l(\boldsymbol{\theta}^{(r)}) + \langle \nabla l(\boldsymbol{\theta}^{(r)}), \boldsymbol{\theta} - \boldsymbol{\theta}^{(r)} \rangle + \frac{\rho^{(r)}}{2} \|\boldsymbol{\theta} - \boldsymbol{\theta}^{(r)}\|^2 \\ + \sum_{t=2}^T \mathcal{P}_{\gamma_1} (|\xi_t|, \lambda_1) + \sum_{i=2}^N \mathcal{P}_{\gamma_2} (\|\boldsymbol{\varsigma}_i\|, \lambda_2),$$

where $\nabla l(\boldsymbol{\theta}^{(r)})$ is the first order derivative of $l(\cdot)$, $\langle \cdot, \cdot \rangle$ is the inner product and $1/\rho^{(r)}$ is the step size. The step size is determined by the line search criterion used in [Gong et al. \(2013\)](#). The detail is provided in Remark 1. Following the GIST algorithm, the problem is equivalent to the following proximal operator problem:

$$\boldsymbol{\theta}^{(r+1)} = \underset{\boldsymbol{\theta}}{\operatorname{argmin}} \frac{1}{2} \|\boldsymbol{\theta} - \mathbf{u}^{(r)}\|^2 + \frac{1}{\rho^{(r)}} \sum_{t=2}^T \mathcal{P}_{\gamma_1}(|\xi_t|, \lambda_1) + \frac{1}{\rho^{(r)}} \sum_{i=2}^N \mathcal{P}_{\gamma_2}(\|\boldsymbol{\varsigma}_i\|, \lambda_2), \quad (13)$$

where $\mathbf{u}^{(r)} = \boldsymbol{\theta}^{(r)} - \nabla l(\boldsymbol{\theta}^{(r)})/\rho^{(r)}$. Since there are no penalties applied to $\boldsymbol{\alpha}$ and $\boldsymbol{\varsigma}_1$, $\boldsymbol{\alpha}^{(r+1)}$ and $\boldsymbol{\varsigma}_1^{(r+1)}$ are updated based on the values in \mathbf{u}^r directly. In particular, $\boldsymbol{\alpha}^{(r+1)} = \mathbf{u}_{[1:q]}^{(r)}$, where $\mathbf{u}_{[1:q]}^{(r)}$ is first q values in $\mathbf{u}^{(r)}$ correspond to $\boldsymbol{\alpha}$. $\boldsymbol{\varsigma}_1^{(r+1)} = \mathbf{u}_{[(q+T):(q+T+p-1)]}^{(r)}$, where $\mathbf{u}_{[(q+T):(q+T+p-1)]}^{(r)}$ is the $q+T$ to $q+T+p-1$ elements, corresponding to $\boldsymbol{\varsigma}_1$ in $\boldsymbol{\theta}$.

To update $\xi_t^{(r+1)}$, $t = 2, \dots, T$, it is equivalent to the following minimization problem,

$$\xi_t^{(r+1)} = \underset{\xi_t}{\operatorname{argmin}} \frac{\rho^{(r)}}{2} (\xi_t - u_{[q+t-1]}^{(r)})^2 + \mathcal{P}_{\gamma_1}(|\xi_t|, \lambda_1),$$

where $u_{[q+t-1]}^{(r)}$ the $(q+t-1)$ th element in $\mathbf{u}^{(r)}$. To update $\boldsymbol{\varsigma}_i^{(r+1)}$, $i = 2, \dots, N$, it is equivalent to the following minimization problem,

$$\boldsymbol{\varsigma}_i^{(r+1)} = \underset{\boldsymbol{\varsigma}_i}{\operatorname{argmin}} \frac{\rho^{(r)}}{2} \|\boldsymbol{\varsigma}_i - \mathbf{u}_{\boldsymbol{\varsigma}_i}^{(r)}\|^2 + \mathcal{P}_{\gamma_2}(\|\boldsymbol{\varsigma}_i\|, \lambda_2),$$

where $\mathbf{u}_{\boldsymbol{\varsigma}_i}^{(r)}$ is the value in $\mathbf{u}^{(r)}$ corresponding to $\boldsymbol{\varsigma}_i$. For MCP ([Zhang, 2010](#)), the solutions for ξ_t and $\boldsymbol{\varsigma}_i$ are

$$\xi_t^{(r+1)} = \begin{cases} \frac{S(u_{[q+t-1]}^{(r)}, \lambda_1/\rho^{(r)})}{1-1/(\gamma_1\rho^{(r)})} & \text{if } |u_{[q+t-1]}^{(r)}| \leq \gamma\lambda, \\ u_{[q+t-1]}^{(r)} & \text{if } |u_{[q+t-1]}^{(r)}| > \gamma\lambda, \end{cases} \quad (14)$$

and

$$\boldsymbol{\varsigma}_i^{(r+1)} = \begin{cases} \frac{S(\mathbf{u}_{\boldsymbol{\varsigma}_i}^{(r)}, \lambda_2/\rho^{(r)})}{1-1/(\gamma_2\rho^{(r)})} & \text{if } \|\mathbf{u}_{\boldsymbol{\varsigma}_i}^{(r)}\| \leq \gamma\lambda, \\ \mathbf{u}_{\boldsymbol{\varsigma}_i}^{(r)} & \text{if } \|\mathbf{u}_{\boldsymbol{\varsigma}_i}^{(r)}\| > \gamma\lambda, \end{cases} \quad (15)$$

where $S(\mathbf{x}, \lambda) = (1 - \lambda/\|\mathbf{x}\|)_+ \mathbf{x}$, and $(x)_+ = x$ if $x > 0$, 0 otherwise.

The estimates $\hat{\boldsymbol{\varsigma}}$ highly depend on the pre-selected tree \mathcal{T} , which has been discussed in [Li and Sang \(2019\)](#), [Zhang et al. \(2022\)](#) and [Lin et al. \(2022\)](#). Figure 1

illustrates two examples of spanning trees. In these two figures, there are two clusters within 25 nodes (locations). In Figure 1a, with a properly constructed tree, there is one edge between two clusters. Then, the graph can be partitioned into two subgraphs by removing the edge between them (the red cross in the figure), representing two clusters. However, in Figure 1b, if the tree is not properly constructed, there are two edges between these two clusters. By removing these two edges (red crosses in the figure), the graph is partitioned into three subgraphs, leading to three clusters.

[Figure 1 about here.]

Here, we propose an adaptive approach to improve the constructed MST, which is not studied in the literature. Consider an initial MST based on neighbors or locations, $\mathcal{T} = (\mathcal{V}, \mathcal{E})$. $\hat{\boldsymbol{\theta}}_{\mathcal{T}}$ is the estimator obtained from minimizing (10) based on the given tree \mathcal{T} . According to the relationship between $\boldsymbol{\beta}$ and $\boldsymbol{\varsigma}$, we can obtain the estimator $\hat{\boldsymbol{\beta}}_{\mathcal{T}} = (\hat{\mathbf{H}}^{-1} \otimes \mathbf{I}_p) \hat{\boldsymbol{\varsigma}}_{\mathcal{T}}$. For any two locations in the original graph \mathcal{G} , we define the following weights based on estimates $\hat{\boldsymbol{\beta}}_{\mathcal{T}}$,

$$w_{ii'} = \begin{cases} \|\hat{\boldsymbol{\beta}}_{\mathcal{T},i} - \hat{\boldsymbol{\beta}}_{\mathcal{T},i'}\|, & \text{if } (i, i') \in \mathcal{E}_0, \\ \infty, & \text{otherwise.} \end{cases} \quad (16)$$

Then, a new MST $\mathcal{T}^* = (\mathcal{V}, \mathcal{E}^*)$ is constructed using the updated weights in (16). In the end, the final estimator $\hat{\boldsymbol{\theta}}^* = (\hat{\boldsymbol{\alpha}}^*, \hat{\boldsymbol{\xi}}^*, \hat{\boldsymbol{\varsigma}}^*)$ is obtained by solving a minimization problem similar to (12) based on the new MST, \mathcal{T}^* . In particular, the penalized likelihood function has the following form

$$\begin{aligned} L(\boldsymbol{\alpha}, \boldsymbol{\eta}, \boldsymbol{\beta}) &= \frac{1}{NT} \sum_{i=1}^N \sum_{t=1}^T \left[-y_{it} \left(\mathbf{z}_{it}^{\top} \boldsymbol{\alpha} + \mathbf{x}_{it}^{\top} \boldsymbol{\beta}_i + \eta_t \right) + n_{it} \exp \left(\mathbf{z}_{it}^{\top} \boldsymbol{\alpha} + \mathbf{x}_{it}^{\top} \boldsymbol{\beta}_i + \eta_t \right) \right] \\ &\quad + \sum_{t=2}^T \mathcal{P}_{\gamma_1} (|\eta_t - \eta_{t-1}|, \lambda_1) + \sum_{(i,i') \in \mathcal{E}^*} \mathcal{P}_{\gamma_2} (\|\boldsymbol{\beta}_i - \boldsymbol{\beta}_{i'}\|, \lambda_2), \end{aligned} \quad (17)$$

where the fusion type penalty is applied to the edges in \mathcal{E}^* . Based on the same arguments, the optimization problem is equivalent to minimizing the following objective function,

$$\begin{aligned} Q^*(\boldsymbol{\theta}) &= \frac{1}{NT} \sum_{i=1}^N \sum_{t=1}^T \left[-y_{it} \left(\mathbf{z}_{it}^{\top} \boldsymbol{\alpha} + \mathbf{x}_{it}^{\top} \mathbf{h}_i^* \boldsymbol{\varsigma} + \mathbf{m}_t^{\top} \boldsymbol{\xi} \right) + n_{it} \exp \left(\mathbf{z}_{it}^{\top} \boldsymbol{\alpha} + \mathbf{x}_{it}^{\top} \mathbf{h}_i^* \boldsymbol{\varsigma} + \mathbf{m}_t^{\top} \boldsymbol{\xi} \right) \right] \\ &\quad + \sum_{t=2}^T \mathcal{P}_{\gamma_1} (|\xi_t|, \lambda_1) + \sum_{i=2}^N \mathcal{P}_{\gamma_2} (\|\boldsymbol{\varsigma}_i\|, \lambda_2), \end{aligned} \quad (18)$$

where $\mathbf{h}_i^* = \tilde{\mathbf{h}}_i^{*\top} \otimes \mathbf{I}_p$, and $\tilde{\mathbf{h}}_i^{*\top}$ is the i th row of $(\tilde{\mathbf{H}}^*)^{-1}$. Here, $\tilde{\mathbf{H}}^* = \begin{pmatrix} \frac{1}{\sqrt{N}} \mathbf{1}^\top \\ \mathbf{H}^* \end{pmatrix}$, and \mathbf{H}^* is the incident matrix corresponding to \mathcal{T}^* . With the estimator $(\hat{\boldsymbol{\alpha}}^*, \hat{\boldsymbol{\xi}}^*, \hat{\boldsymbol{\varsigma}}^*) = \arg \min_{\boldsymbol{\theta}} Q^*(\boldsymbol{\theta})$, the estimated time effect and regression coefficients are $\hat{\boldsymbol{\eta}}^* = \mathbf{M} \hat{\boldsymbol{\xi}}^*$ and $\hat{\boldsymbol{\beta}}^* = (\tilde{\mathbf{H}}^* \otimes \mathbf{I}_p)^{-1} \hat{\boldsymbol{\varsigma}}^* = (\tilde{\mathbf{H}}^{*-1} \otimes \mathbf{I}_p) \hat{\boldsymbol{\varsigma}}^*$.

In summary, the computational algorithm for a given λ_1 and a given λ_2 is outlined as follows:

Algorithm 1 Adaptive algorithm

Require: : Initialize \mathcal{T} and $\boldsymbol{\theta}^{(0)}$.

- 1: **for** $r = 0, 1, 2, \dots$ **do**
 - 2: Initialize $\rho^{(r)} = 1$.
 - 3: **repeat**
 - 4: Update $\boldsymbol{\theta}^{(r+1)}$ based on (13), (14) and (15).
 - 5: $\rho^{(r+1)} = 2\rho^{(r)}$.
 - 6: **until** some line search criterion is satisfied.
 - 7: **if** convergence criterion is met **then**
 - 8: Stop and get the estimates $\hat{\boldsymbol{\theta}}_{\mathcal{T}}$.
 - 9: **else**
 - 10: $r = r + 1$
 - 11: **end if**
 - 12: **end for**
 - 13: Obtain the updated MST, \mathcal{T}^* , based on $\hat{\boldsymbol{\theta}}_{\mathcal{T}}$.
 - 14: Repeat steps 1 - 12 to obtain the final estimates based on \mathcal{T}^* .
-

Remark 1. *Gong et al. (2013) discussed the linear search criterion in detail. Here we follow their procedure, that is $Q(\boldsymbol{\theta}^{(r+1)}) \leq Q(\boldsymbol{\theta}^{(r)}) - \frac{\sigma}{2} \rho^{(r)} \|\boldsymbol{\theta}^{(r+1)} - \boldsymbol{\theta}^{(r)}\|$, where $\sigma = 10^{-5}$ as used in Gong et al. (2013). And the convergence criterion we use here is $\max\{|\theta_t^{(r+1)} - \theta_t^{(r)}|\} < 10^{-4}$.*

Remark 2. *The initial values can be obtained by fitting a Poisson regression model with location-specific effects $\boldsymbol{\beta}_i$ and individual time effect η_t .*

Recall that by changing the values of λ_1 and λ_2 , we can obtain the estimates of the number of changed points \hat{J} and the number of clusters \hat{K} . Following the

literature [Ma et al. \(2020\)](#), λ_1 and λ_2 are selected based on minimizing the following modified BIC,

$$BIC(\lambda_1, \lambda_2) = 2l_0(\hat{\boldsymbol{\alpha}}, \hat{\boldsymbol{\eta}}, \hat{\boldsymbol{\beta}}) + C_N \log(NT)(\hat{K}p + \hat{J}), \quad (19)$$

where $l(\cdot)$ is the negative loglikelihood in (4), \hat{J} is the estimated number of changed points, \hat{K} is the estimated number of clusters, p is the dimension of \boldsymbol{x} , and $C_N = \log(Np + T - 1)$.

A two-step procedure is implemented to select these two tuning parameters. First, we set $\lambda_2 = 0$ and select λ_1 for a given tree \mathcal{T} based on BIC in (19). Specifically, λ_1 will be chosen from a grid of values of λ_1 . Second, given the selected λ_1 , for each λ_2 , we implement the algorithm described in Algorithm 1. Then, λ_2 will be selected based on the BIC in (19). Thus, we can have the final estimates.

3 Theoretical properties

In this section, we study the theoretical properties of our proposed estimator. We will study the properties in two steps. In the first step, we will present the theoretical properties for a given tree \mathcal{T} . In the second step, we will provide the properties for the estimator based on the adaptive tree \mathcal{T}^* .

First, we will introduce some notations. Let $\boldsymbol{\alpha}^0, \boldsymbol{\eta}^0, \boldsymbol{\beta}^0$ be the true parameters vectors, where $\boldsymbol{\beta}^0 = (\boldsymbol{\beta}_1^0, \dots, \boldsymbol{\beta}_N^0)$, and the true cluster structure is $\mathcal{C}^0 = \{\mathcal{C}_k^0\}_{k=1}^K$, where K is the number of clusters. For a given MST, $\mathcal{T} = (\mathcal{V}, \mathcal{E})$, define $\mathbb{C}_{\mathcal{T}} = \{(i, i') \in \mathcal{E} : \boldsymbol{\beta}_i^0 \neq \boldsymbol{\beta}_{i'}^0\}$, which corresponds to the edges in \mathcal{T} and the nodes (locations) are not in the same cluster. Then by removing $|\mathbb{C}_{\mathcal{T}}|$ number of edges, we can obtain $K_{\mathcal{T}} \equiv |\mathbb{C}_{\mathcal{T}}| + 1$ number of clusters, and the corresponding cluster structure is denoted as $\mathcal{C}_{\mathcal{T}}$. Note that, $K_{\mathcal{T}}$ may not be the same as K as discussed in Figure 1. Let $\boldsymbol{\theta}_{\mathcal{T}} = (\boldsymbol{\alpha}^{\top}, \boldsymbol{\xi}^{\top}, \boldsymbol{\varsigma}^{\top})^{\top}$ be the transformed parameter vector depending on \mathcal{T} . Recall that $\boldsymbol{\varsigma}_i$ represents $\boldsymbol{\beta}_i - \boldsymbol{\beta}_{i'}$ for $(i, i') \in \mathcal{E}$, if the nonzero $\boldsymbol{\varsigma}_i$ can be identified, then the corresponding cluster structure $\mathcal{C}_{\mathcal{T}}$ can then be identified. As discussed above, if MST is properly constructed, such that by removing $|\mathbb{C}_{\mathcal{T}}|$ edges, we can recover the true cluster structure \mathcal{C}^0 . Because of the one-to-one mapping relationship between $\boldsymbol{\varsigma}$ and $\boldsymbol{\beta}$, $\boldsymbol{\xi}$ and $\boldsymbol{\eta}$, thus estimating $\boldsymbol{\varsigma}$ and $\boldsymbol{\xi}$ is equivalent to estimating $\boldsymbol{\beta}$ and $\boldsymbol{\eta}$. Thus, we will focus on the properties of $\hat{\boldsymbol{\theta}}$.

Let $\boldsymbol{\theta}_{\mathcal{T},0}$ be the transformed true parameters vector based on $\boldsymbol{\alpha}^0, \boldsymbol{\eta}^0, \boldsymbol{\beta}^0$ for a given tree \mathcal{T} . Let $\mathcal{S}_N = \{i \in \{2, 3, \dots, N\}; \|\boldsymbol{\varsigma}_i\| \neq 0\}$ and $\mathcal{N}_N = \{i \in \{2, 3, \dots, N\}, \|\boldsymbol{\varsigma}_i\| = 0\}$, which represent the nonzero and zero sets of $\boldsymbol{\varsigma}_i$, for $i = 2, 3, \dots, N$ and have penalties applied in the objective function. Denote $\boldsymbol{\varsigma}_{(1)}$ and $\boldsymbol{\varsigma}_{(2)}$ as the parameter

vectors for \mathcal{S}_N and \mathcal{N}_N , respectively. Let \mathcal{S}_T and \mathcal{N}_T be the nonzero and zero sets of ξ_t . And denote $\boldsymbol{\xi}_{(1)}$ and $\boldsymbol{\xi}_{(2)}$ as the parameter vectors for \mathcal{S}_T and \mathcal{N}_T , respectively. Furthermore, denote $\boldsymbol{\theta}_{\mathcal{T},0} = (\boldsymbol{\theta}_{\mathcal{T},1,0}^\top, \boldsymbol{\theta}_{\mathcal{T},2,0}^\top)^\top$, where $\boldsymbol{\theta}_{\mathcal{T},1,0} = (\boldsymbol{\alpha}^\top, \boldsymbol{\varsigma}_1^\top, \boldsymbol{\varsigma}_{(1)}^\top, \boldsymbol{\xi}_{(1)}^\top)^\top$ is the true nonzero parameters vector and $\boldsymbol{\theta}_{\mathcal{T},2,0} = \mathbf{0}$ is the zero parameters vector. $d = 2^{-1} \min \{ \|\boldsymbol{\varsigma}_i\|, i \in \mathcal{S}_N, |\xi_t|, t \in \mathcal{S}_T \}$, represents the signal.

Let $\tilde{\mathbf{X}} = \text{diag}(\mathbf{x}_1, \mathbf{x}_2, \dots, \mathbf{x}_N)$, where $\mathbf{x}_i = (x_{i1}, \dots, x_{iT})^\top$, $\mathbb{X} = \tilde{\mathbf{X}} (\tilde{\mathbf{H}}^{-1} \otimes \mathbf{I}_p)$ and $\mathbb{M} = \mathbf{1}_N \otimes \begin{pmatrix} \mathbf{0}_{T-1}^\top \\ \mathbf{M} \end{pmatrix}$. Let $\mathbb{U} = (\mathbf{Z}, \mathbb{X}, \mathbb{M}) = (\mathbb{U}_1, \mathbb{U}_2)$, where \mathbb{U}_1 is the design matrix corresponding to $\boldsymbol{\theta}_{1,0}$, and \mathbb{U}_2 is the design matrix corresponding $\boldsymbol{\theta}_{2,0}$. For any positive numbers, x_T and y_T , $x_T \gg y_T$ means that $x_T^{-1}y_T = o(1)$.

Below are the assumptions.

- (C1) The design matrix \mathbb{U} satisfies that $\lambda_{\min} \left[\frac{1}{NT} \mathbb{U}_1^\top \mathbb{U}_1 \right] \geq c_1$ and $\lambda_{\max} \left[\frac{1}{NT} \mathbb{U}_1^\top \mathbb{U}_1 \right] \leq c_2$ for some positive constants c_1 and c_2 , where $\lambda_{\min}(\cdot)$ and $\lambda_{\max}(\cdot)$ are the corresponding minimum and maximum eigenvalues respectively. In addition, $\|\mathbf{x}_{it}\|$ is bounded.
- (C2) $\boldsymbol{\mu}(\boldsymbol{\delta})$ is bounded by some constants M_1 and M_2 with $M_1 < M_2$ for $\boldsymbol{\delta} \in \mathcal{N}_0$, where $\boldsymbol{\mu}(\boldsymbol{\delta})$ is the vector of expected values of y_{it} for $i = 1, \dots, N$ and $t = 1, \dots, T$, $\mathcal{N}_0 = \{ \boldsymbol{\delta} \in \mathbb{R}^s : \|\boldsymbol{\delta} - \boldsymbol{\theta}_{1,0}\|_\infty \leq d \}$ and s is the dimension $\boldsymbol{\theta}_{1,0}$.
- (C3) $d \gg \max(\lambda_1, \lambda_2)$, $\lambda_1 \gg \max \{ \sqrt{s/N_0}, u/\sqrt{N_0} \}$, and $\lambda_2 \gg \max \{ \sqrt{s/N_0}, u/\sqrt{N_0} \}$, where $u \gg \sqrt{\log N_0}$, $uN_0^{-1/2} = o(1)$ and $N_0 = NT$.
- (C4) For any two locations i and i' in the given connected network $\mathcal{G} = (\mathcal{V}, \mathcal{E}_0)$, if they are from the same cluster, then there exists a path connecting them such that all locations on the path belong to the same cluster.

Condition (C1) is a commonly used condition for the design matrix in penalized problems (Fan and Lv, 2011; Wang et al., 2023b). Conditions (C2) and (C3) for tuning parameters λ_1 , λ_2 and the minimum signal d guarantee the oracle properties of the estimator, which are adjusted based on those in Fan and Lv (2011). Condition (C4) is used in Zhang et al. (2022) to ensure that the locations within the same cluster are not separated by other clusters in the graph \mathcal{G} . We can use a full graph with all pairwise connections or based on adjacency matrices, where the adjacency matrix presents the neighborhood structure of locations. In particular, if location i and i' are neighbors, then $(i, i') \in \mathcal{E}_0$. Moreover, based on the neighborhood structure, we can also define a graph based on k -nearest neighbors. Condition (C4) guarantees

that by removing inner-cluster connections, the original graph can be reduced to K subgraphs, which correspond to K clusters.

Theorem 1 shows the theoretical properties of the estimator based on the objective function in (11) for a given tree \mathcal{T} . The proof is provided in Appendix B.1.

Theorem 1. *Assume conditions (C1)-(C3) hold, p and q are fixed. Then there exists a strict local minimizer $\hat{\boldsymbol{\theta}} = (\hat{\boldsymbol{\theta}}_1^\top, \hat{\boldsymbol{\theta}}_2^\top)^\top$ of $Q(\boldsymbol{\theta})$ in (11) such that $\hat{\boldsymbol{\theta}}_2 = \mathbf{0}$ with probability tending to 1 as $T \rightarrow \infty$ and $\|\hat{\boldsymbol{\theta}}_1 - \boldsymbol{\theta}_{\mathcal{T},1,0}\| = O_P(\sqrt{s/N_0})$.*

Remark 3. *Theorem 1 gives the sparsity and consistency of the estimator for a given tree \mathcal{T} . The sparsity property indicates that the cluster structure $\mathcal{C}_{\mathcal{T}}$ based on \mathcal{T} can be recovered. But $\mathcal{C}_{\mathcal{T}}$ may not be the same as \mathcal{C}^0 .*

Lemma 2 in Appendix A.2 discussed the property of the updated MST, \mathcal{T}^* , constructed based on weights in (16). Lemma 2 implies that the cluster structure $\mathcal{C}_{\mathcal{T}^*}$ based on \mathcal{T}^* will be the same as the true cluster structure \mathcal{C}^0 with probability approaching 1. Under \mathcal{T}^* , we have the following theorem to summarize the theoretical properties of the adaptive tree based estimator based on (18). The proof is provided in Appendix B.2. Let \mathcal{S}_N^* be the index of nonzero ς_i based on \mathcal{T}^* , and $\hat{\mathcal{S}}_N^*$ is the estimated index.

Theorem 2. *Assume conditions (C1) - (C4) hold, p and q are fixed. Based on the MST, \mathcal{T}^* , the adaptive tree based estimator $\hat{\boldsymbol{\theta}}_1$ satisfies that $\|\hat{\boldsymbol{\theta}}_1 - \boldsymbol{\theta}_{1,0}\| = O_P(\sqrt{s/N_0})$. Furthermore, the sparsity property is that $\lim_{T \rightarrow \infty} P(\hat{\mathcal{S}}_N^* = \mathcal{S}_N^*) = 1$ and $\lim_{T \rightarrow \infty} P(\hat{\mathcal{S}}_T = \mathcal{S}_T) = 1$.*

Remark 4. *In Theorem 2, $\boldsymbol{\theta}_{1,0}$ depends on the structure of \mathcal{T}^* . Due to the one-to-one mapping relationship between $\boldsymbol{\varsigma}$ and $\boldsymbol{\beta}$, when the sparsity structure of $\boldsymbol{\varsigma}$ is recovered, the cluster structure of $\boldsymbol{\beta}$, \mathcal{C}^0 , is also recovered.*

4 Simulation

In this section, we use several simulation examples to evaluate the performance of our proposed estimator. First, we compare our proposed method to the traditional spatial scan approaches in Section 4.1 when the number of clusters is 2. Then, we evaluate our proposed method for different setups in Section 4.2.

4.1 Comparison to spatial scan approaches

In this section, we will compare our proposed method to spatial scan approaches when the number of clusters is 2. To evaluate the performance of recovering cluster structure, we use the estimated number of clusters (\hat{K}) and adjusted Rand Index (ARI)(Hubert and Arabie, 1985). ARI is widely used to measure the agreement of two partitions. The largest value of ARI is 1, and the larger, the better.

We simulate our data from the model in (3) with clustered intercepts. The population value n_{it} is generated from a lognormal distribution with parameters of center 10 and standard deviation 0.7. z_{it} 's, for $i = 1, 2, \dots, N$ and $t = 1, \dots, T$, are simulated from the standard normal distribution, and the regression coefficient $\alpha = 0.5$. For time effect η_t , we consider one change point with $\eta_t = 0$ for $t = 1, \dots, 10$ and $\eta_t = -0.5$ for $t = 11, \dots, T = 20$. For location-specific effect β_i , we consider two clusters with $N = 100$ and the two spatial structures as shown in Figure 2. Figure 2a is a 10×10 grid lattice and Figure 2b contains 100 random locations uniformly generated from $(-1, 1)$. In both structures, the center cluster is smaller than the outside cluster. Specifically, $\beta_i = -7$ if i is in the smaller cluster and $\beta_i = -7.5$ if i is in the big cluster.

[Figure 2 about here.]

We compare our proposed adaptive method (denoted as “adaptive”) with several spatial scan statistics for functional data implemented in the R package *HDSpatialScan* (Frévent et al., 2022), including nonparametric functional scan statistic (NPFSS) (Smida et al., 2022), parametric functional scan statistic (PFSS) (Frévent et al., 2021), distribution-free functional scan statistic (DFSS) (Frévent et al., 2021) and univariate rank-based functional scan statistic (URBFSS) (Frévent et al., 2023). Besides these approaches, we also consider two methods in the R package *scanstatistics* (Allevius, 2018), one is the space-time permutation scan statistic (PSS) (Kulldorff et al., 2005) and the other one is population-based Poisson scan statistic (PPSS)(Kulldorff, 2001). We also consider the method using MST based on locations, denoted as “tree”. Tables 1 and 2 show the average ARI and average estimated number of cluster \hat{K} based on 100 simulations for different methods, along with standard deviation values in parentheses. We observe that approaches based on scan statistics cannot identify the cluster structure well. This is because these approaches do not consider the effects of covariates and the changes in the temporal domain. When comparing the adaptive method to the tree based approach, we can have better performance in terms of estimating cluster structure.

[Table 1 about here.]

[Table 2 about here.]

4.2 Evaluation of model performance

In this section, we will evaluate the performance of our proposed adaptive approach when the number of clusters is 5, and the number of change points is 2. We will compare the adaptive approach to the tree based approach. Besides the estimated number of clusters \hat{K} and ARI, we also report the estimated number of changed points (\hat{J}) and the F1 score (Sasaki, 2007) to evaluate the performance of detecting changed points. F1 score measures classification accuracy (changed or nonchanged) with the highest value of 1 and the smallest value of 0. The higher the value of the F1 score is, the better the accuracy of temporal trend detection is. The F1 score is defined as $F1 = \frac{2PR}{P+R}$, where P is precision and R is recall. To evaluate the estimation accuracy, we report the root mean square error (RMSE) for estimating β , η and α . RMSE is defined as $\sqrt{\frac{1}{|\theta|} \|\hat{\theta} - \theta\|^2}$, where θ can be β , η or α , $\hat{\theta}$ is an estimate of θ and $|\theta|$ is the dimension of θ .

Similar to the setup in Section 4.1, we consider two spatial cluster structures: one is a grid lattice, and the other one is based on random locations. Figure 3 shows the two underlying true cluster structures.

[Figure 3 about here.]

We simulate data as follows: let $\mathbf{x}_{it} = [1, x_{it}]^\top$ with x_{it} 's are generated from $\sim N(0, 1)$, and z_{it} 's are generated from $N(0, 1)$, for $i = 1, 2, \dots, 100$ and $t = 1, 2, \dots, 25$. For model parameters, we set $\alpha = 0.5$, and β_i takes two set of parameters for five clusters $\mathcal{C}_1, \mathcal{C}_2, \mathcal{C}_3, \mathcal{C}_4$ and \mathcal{C}_5 :

Setting 1: $\beta_i = (-8, -1)^T$ if $i \in \mathcal{C}_1$; $\beta_i = (-7.7, -0.5)^T$ if $i \in \mathcal{C}_2$; $\beta_i = (-7.5, 0)^T$ if $i \in \mathcal{C}_3$; $\beta_i = (-7.2, 0.5)^T$ if $i \in \mathcal{C}_4$; $\beta_i = (-7, 1)^T$ if $i \in \mathcal{C}_5$;

Setting 2: $\beta_i = (-8, -0.5)^T$ if $i \in \mathcal{C}_1$; $\beta_i = (-7.7, -0.25)^T$ if $i \in \mathcal{C}_2$; $\beta_i = (-7.5, 0)^T$ if $i \in \mathcal{C}_3$; $\beta_i = (-7.2, 0.25)^T$ if $i \in \mathcal{C}_4$; $\beta_i = (-7, 0.5)^T$ if $i \in \mathcal{C}_5$.

The cluster difference of setting 2 is smaller than that of setting 1. We assume there are 2 changed points, one is at $t = 5$ with a change from 0 to -0.5, and the other one is at $t = 15$ with a change from -0.5 to -0.8.

Table 3 and Table 4 show the average ARI, \hat{K} , F1 score and \hat{J} over 100 simulations, along with standard deviations in parentheses, for two different spatial cluster structures. Figure 4 and Figure 5 show the RMSE for estimating α , β and η under two spatial cluster structures. It can be seen that the structure of trees does not affect change point detection but significantly affects cluster identification. The

adaptive method has larger ARI values and smaller RMSE values compared to the tree based approach. The tree based approach tends to identify more clusters. This is because that the initial MST may not reflect the true spatial structure.

[Table 3 about here.]

[Table 4 about here.]

[Figure 4 about here.]

[Figure 5 about here.]

5 Real data analysis

In this section, we apply our proposed method to the data from Surveillance, Epidemiology, and End Results (SEER) program (SEER, 2023; Duggan et al., 2016). SEER program provides cancer statistics for the US population, with data collected in several states since 1973. Currently, there are 22 registries, including states and metropolitan areas, which can cover approximately 47.9% of the U.S. population. SEER data is widely used in different studies for different cancers, such as breast cancer (Guha et al., 2022), lung cancer (Tolwin et al., 2020), and colon and rectum cancer (Daly and Paquette, 2019). There are also some existing studies about cluster detection in SEER data. For example, Geng and Hu (2022) conducted an analysis of personal-level data on respiratory cancer to find clusters in Louisiana counties. Chernyavskiy et al. (2019) used multilevel age-period-cohort models to analyze the heterogeneity of colon and rectum cancer incidence across different counties and age groups. Exploring the spatial cluster structure of incidence can help to allocate resources for interventions and enhance the understanding of spatially varying risk factors (Chernyavskiy et al., 2019; Amin et al., 2019).

As an illustration, we consider colon and rectum cancer in Iowa from 1995 to 2020. The response variable y_{it} is the number of deaths with an age greater than 30 in each county. The covariate is poverty from the Small Area Income and Poverty Estimates (SAIPE) Program. The poverty data are obtained from the R package *censusapi*, which has a complete time series record from 1995 to 2020. We consider the following model for the 99 counties in Iowa from the year 2006 to 2020,

$$y_{it} \sim \text{Poisson}(n_{it}\mu_{it}), \quad \log \mu_{it} = z_{it}\alpha + \beta_i + \eta_t, \quad (20)$$

where n_{it} is the population for age greater than 30 for county i at year t , z_{it} presents the estimated poverty for county i at year t from SAIPE, α is the common regression

coefficient, β_i the county effect, and η_t is the time effect. Our goal is to find the cluster structure of β_i , and detect change points of η_t .

Figure 6 gives the estimated cluster structure of county effects. There is one isolated county, Johnson County, which has the smallest estimated $\hat{\beta}_i = -8.214$ with a standard error of 0.0537. This county is the county where Iowa City and the University of Iowa are located. The cluster with $\hat{\beta}_i = -8.021$ with a standard error of 0.0241 has the second smallest county effect. This cluster includes five counties: Madison, Warren, Dallas, Polk, and Story. Among these five counties, Des Moines is the capital of Iowa, and it is in Polk County. Ames is in Story County; it is the city where Iowa State University is. Besides these two small clusters, there are two larger clusters that have larger county effects. The two counties with the largest county effect are Mitchell and Howard, which shows a difference between these two counties and the surrounding counties. The heterogeneity of county effects suggests more resources can be allocated to counties with larger death rates.

[Figure 6 about here.]

Two changed points are detected. One is in 2004, changed from 0 to -0.2081 with a standard error of 0.02; the other one is in 2012, changed from -0.2081 to -0.3714 with a standard error of 0.0202. The estimated negative changes indicate that the death rate has large declines in 2004 and 2012.

6 Conclusion and discussions

In this article, we proposed a new method for clustering locations based on covariate effects and identifying temporal change points for count data based on a Poisson regression model. To achieve the goal, we designed a doubly penalized likelihood approach. In the proposed approach, an adaptive minimum spanning tree (MST) was used to identify spatial clusters, and a fused penalty was used to detect change points. In the simulation study, we used several numerical examples to investigate the performance of the proposed approach. The numerical results showed that the proposed approach outperforms traditional scan statistics in recovering spatial structures. We also found that the adaptive MST can perform better than a random tree in terms of recovering spatial cluster structure.

The idea of the proposed approach can be extended to semiparametric or non-parametric regression models, which can model the effects of covariates more flexibly, as discussed in linear regression models (Liu and Lin, 2019). Besides this, there is a potential to explore the patient level in the SEER data to identify the heterogeneity for both individual patient and spatial levels.

Appendix

A Lemmas

In this part, we introduce two lemmas, which will be used later in the proof of Theorem 1 and Theorem 2.

A.1 Lemma 1

Some notations are defined as below before introducing Lemma 1.

Denote $\hat{\boldsymbol{\theta}}$ as an estimator of $\boldsymbol{\theta}$.

Let $\hat{\mathcal{S}}_N = \{i \in \{2, 3, \dots, N\}; \|\hat{\boldsymbol{\zeta}}_i\| \neq 0\}$, and $\hat{\mathcal{N}}_N = \{i \in \{2, 3, \dots, N\}; \|\hat{\boldsymbol{\zeta}}_i\| = 0\}$ be the nonzero and zero sets of estimates $\hat{\boldsymbol{\zeta}}$. Denote $\hat{\boldsymbol{\zeta}}_{(1)}$ and $\hat{\boldsymbol{\zeta}}_{(2)}$ as the parameter vectors for $\hat{\mathcal{S}}_N$ and $\hat{\mathcal{N}}_N$, respectively. Similarly, $\hat{\mathcal{S}}_T = \{i \in \{2, 3, \dots, T\}; |\hat{\xi}_i| \neq 0\}$, and $\hat{\mathcal{N}}_T = \{i \in \{2, 3, \dots, T\}; |\hat{\xi}_i| = 0\}$ be the nonzero and zero sets of estimates $\hat{\boldsymbol{\xi}}$. And denote $\hat{\boldsymbol{\xi}}_{(1)}$ and $\hat{\boldsymbol{\xi}}_{(2)}$ as the parameter vectors for $\hat{\mathcal{S}}_T$ and $\hat{\mathcal{N}}_T$, respectively.

Recall that the first column of $\tilde{\mathbf{H}}^{-1}$ is $\frac{1}{\sqrt{N}}\mathbf{1}$, then the column in \mathbb{X} corresponds to $\boldsymbol{\varsigma}_1$ is $\mathbf{X}^* = (\mathbf{x}_1^\top, \mathbf{x}_2^\top, \dots, \mathbf{x}_N^\top)^\top$. Let \mathbb{X}_1 and \mathbb{X}_2 denote the submatrices of \mathbb{X} formed by columns $\hat{\mathcal{S}}_N$ and $\hat{\mathcal{N}}_N$. \mathbb{M}_1 and \mathbb{M}_2 denote the submatrices of \mathbb{M} formed by columns $\hat{\mathcal{S}}_T$ and $\hat{\mathcal{N}}_T$.

For MCP penalty, we have

$$\mathcal{P}'_\gamma(t, \lambda) = \begin{cases} \lambda \text{sign}(t) - \frac{t}{\gamma} = \left(\lambda - \frac{|t|}{\gamma}\right) \text{sign}(t) & |t| \leq \gamma\lambda, \\ 0 & |t| > \gamma\lambda, \end{cases}$$

and $\mathcal{P}'_\gamma(0+; \lambda) = \lambda$. We also define $\kappa_\gamma(\boldsymbol{\theta})$ as follows,

$$\kappa_\gamma(\boldsymbol{\theta}) = \lim_{\epsilon \rightarrow 0+} \max_j \sup_{0 < t_1 < t_2 \in (|\theta_j| - \epsilon, |\theta_j| + \epsilon)} - \frac{\mathcal{P}'_\gamma(t_2) - \mathcal{P}'_\gamma(t_1)}{t_2 - t_1},$$

which corresponds to the second order derivative of $-\mathcal{P}_\gamma(t; \lambda)$ when the second order derivative exists. Note that, for MCP, the second-order derivative does not exist for a finite number of values of t , they are 0, and $\gamma\lambda$. When $|\theta_j| > \gamma\lambda$, then $\kappa_\gamma(\boldsymbol{\theta}) = 0$.

Let $\mathbf{b} = \mathbf{Z}\boldsymbol{\alpha} + \mathbb{X}\boldsymbol{\varsigma} + \mathbb{M}\boldsymbol{\xi}$, $\boldsymbol{\mu}(\boldsymbol{\theta}) = (n_{it} \exp(b_{it}))_{1 \leq i \leq N, 1 \leq t \leq T}$, and $\boldsymbol{\Sigma}(\boldsymbol{\theta}) = \text{diag}(n_{it} \exp(b_{it}); 1 \leq i \leq N, 1 \leq t \leq T)$, $\boldsymbol{\mu}(\boldsymbol{\theta})$ corresponds to the expected values vector of y_{it} for $i = 1, \dots, N$ and $t = 1, \dots, T$, and $\boldsymbol{\Sigma}(\boldsymbol{\theta})$ is the covariance matrix. We have the following lemma that gives sufficient conditions on the strict local minimizer of $Q(\boldsymbol{\theta})$. The proof follows that in [Fan and Lv \(2011\)](#).

Lemma 1. $\hat{\boldsymbol{\theta}}$ is a strict local minimizer of $Q(\boldsymbol{\theta})$ if

$$\frac{1}{NT} \mathbf{Z}^\top (\mathbf{y} - \boldsymbol{\mu}(\hat{\boldsymbol{\theta}})) = \mathbf{0} \quad (21)$$

$$\frac{1}{NT} \mathbf{X}^{*\top} (\mathbf{y} - \boldsymbol{\mu}(\hat{\boldsymbol{\theta}})) = \mathbf{0} \quad (22)$$

$$\frac{1}{NT} \mathbb{X}_1^\top (\mathbf{y} - \boldsymbol{\mu}(\hat{\boldsymbol{\theta}})) - \left(\frac{\hat{\boldsymbol{\zeta}}_i}{\|\hat{\boldsymbol{\zeta}}_i\|} \mathcal{P}'_{\gamma_2} (\|\hat{\boldsymbol{\zeta}}_i\|; \lambda_2); i \in \hat{\mathcal{S}}_N \right) = \mathbf{0} \quad (23)$$

$$\frac{1}{NT} \mathbb{M}_1^\top (\mathbf{y} - \boldsymbol{\mu}(\hat{\boldsymbol{\theta}})) - \left(\mathcal{P}'_{\gamma_1} (\hat{\xi}_t; \lambda_1); t \in \hat{\mathcal{S}}_T \right) = \mathbf{0} \quad (24)$$

$$\max_{i \in \hat{\mathcal{N}}_N} \left\| \frac{1}{NT} \mathbb{X}_{2(i)}^\top (\mathbf{y} - \boldsymbol{\mu}(\hat{\boldsymbol{\theta}})) \right\| < \mathcal{P}'_{\gamma_2} (0+) = \lambda_2 \quad (25)$$

$$\left\| \frac{1}{NT} \mathbb{M}_2^\top (\mathbf{y} - \boldsymbol{\mu}(\hat{\boldsymbol{\theta}})) \right\|_\infty < \mathcal{P}'_{\gamma_1} (0+) = \lambda_1 \quad (26)$$

$$\lambda_{\min} \left(\frac{1}{NT} \mathbf{Z}^\top \boldsymbol{\Sigma}(\hat{\boldsymbol{\theta}}) \mathbf{Z} \right) > 0 \quad (27)$$

$$\lambda_{\min} \left(\frac{1}{NT} \mathbf{X}^{*\top} \boldsymbol{\Sigma}(\hat{\boldsymbol{\theta}}) \mathbf{X}^{*\top} \right) > 0 \quad (28)$$

$$\lambda_{\min} \left(\frac{1}{NT} \mathbb{X}_1^\top \boldsymbol{\Sigma}(\hat{\boldsymbol{\theta}}) \mathbb{X}_1 \right) > \kappa_{\gamma_2} \quad (29)$$

$$\lambda_{\min} \left(\frac{1}{NT} \mathbb{M}_1^\top \boldsymbol{\Sigma}(\hat{\boldsymbol{\theta}}) \mathbb{M}_1 \right) > \kappa_{\gamma_1} \quad (30)$$

where $\mathbb{X}_{2(i)}$ corresponds to the submatrix of \mathbb{X}_2 formed by $\hat{\boldsymbol{\zeta}}_i$ for $i \in \hat{\mathcal{S}}_N$.

Proof. First, we write the likelihood function in (4) as $l(\boldsymbol{\theta})$ in the following way

$$l(\boldsymbol{\theta}) = \frac{1}{NT} \left(-\mathbf{y}^\top (\mathbf{Z}\boldsymbol{\alpha} + \mathbb{X}\boldsymbol{\varsigma} + \mathbb{M}\boldsymbol{\xi}) + \mathbf{1}^\top \boldsymbol{\mu}(\boldsymbol{\theta}) \right) = \frac{1}{NT} \left(-\mathbf{y}^\top \mathbb{U}\boldsymbol{\theta} + \mathbf{1}^\top \boldsymbol{\mu}(\boldsymbol{\theta}) \right). \quad (31)$$

Then, the first order derivative and the second order derivative have the following forms,

$$\begin{aligned} \nabla l(\boldsymbol{\theta}) &= -\frac{1}{NT} \mathbb{U}^\top (\mathbf{y} - \boldsymbol{\mu}(\boldsymbol{\theta})), \\ \nabla^2 l(\boldsymbol{\theta}) &= \frac{1}{NT} \mathbb{U}^\top \boldsymbol{\Sigma}(\boldsymbol{\theta}) \mathbb{U}. \end{aligned}$$

Recall $\mathbb{U} = (\mathbf{Z}, \mathbb{X}, \mathbb{M}) = (\mathbf{Z}, \mathbf{X}^*, \mathbb{X}_1, \mathbb{X}_2, \mathbb{M}_1, \mathbb{M}_2)$, $\hat{\boldsymbol{\theta}}$ is a local minimizer of the objective function $Q(\boldsymbol{\theta})$ if it satisfies the Karush-Kuhn-Tucker (KKT) conditions, that is

$$\frac{1}{NT} \mathbb{U}^\top (\mathbf{y} - \boldsymbol{\mu}(\hat{\boldsymbol{\theta}})) - \mathbf{v} = \mathbf{0}.$$

For $\boldsymbol{\alpha}$ and $\boldsymbol{\varsigma}_1$, there are no penalty terms, thus the corresponding $v_j = 0$. Thus, we have conditions (21) and (22). For $i \in \hat{\mathcal{S}}_N$, $\|\hat{\boldsymbol{\varsigma}}_i\| \neq 0$, the corresponding values in \boldsymbol{v} is $\frac{\hat{\boldsymbol{\varsigma}}_i}{\|\hat{\boldsymbol{\varsigma}}_i\|} \mathcal{P}'_{\gamma_2}(\|\hat{\boldsymbol{\varsigma}}_i\|; \lambda_2)$; for $t \in \hat{\mathcal{S}}_T$, the corresponding element in \boldsymbol{v} is $\mathcal{P}'_{\gamma_1}(\xi_t; \lambda_1)$. Thus, we have conditions (23) and (24). For $i \in \hat{\mathcal{N}}_N$, the elements in \boldsymbol{v} are $\|\boldsymbol{v}_i\|$, which is any value between $[-\mathcal{P}'(0+), \mathcal{P}'(0+)] = [-\lambda_2, \lambda_2]$ (Loh and Wainwright, 2015), and for $t \in \hat{\mathcal{N}}_T$, the element in \boldsymbol{v} is between $[-\lambda_1, \lambda_1]$. Thus, we have the conditions in (25) and (26).

Now consider the second order conditions. For the parameters without penalty terms, we have (27) and (28). For $\hat{\boldsymbol{\varsigma}}_{(1)}$ and $\hat{\boldsymbol{\xi}}_{(1)}$, we have

$$\lambda_{\min} \left(\frac{1}{NT} \mathbb{X}_1^\top \boldsymbol{\Sigma}(\hat{\boldsymbol{\theta}}) \mathbb{X}_1 \right) \geq \kappa_{\gamma_2}, \quad (32)$$

$$\lambda_{\min} \left(\frac{1}{NT} \mathbb{M}_1^\top \boldsymbol{\Sigma}(\hat{\boldsymbol{\theta}}) \mathbb{M}_1 \right) \geq \kappa_{\gamma_1}. \quad (33)$$

Note that (32) and (33) are nonstrict inequalities. Next, we will show that strict inequalities are sufficient conditions for strict local minimizer.

First consider the $Q(\boldsymbol{\theta})$ on the $\|\hat{\boldsymbol{\theta}}\|_0$ dimensional subspace $\mathcal{B} = \{\boldsymbol{\theta} \in \mathbb{R}^{q+Np+T-1} : \boldsymbol{\theta}_c = \mathbf{0}\}$, where $\boldsymbol{\theta}_c$ is the subvector of $\boldsymbol{\theta}$ formed by components in $\hat{\mathcal{N}}_N$ and $\hat{\mathcal{N}}_T$. Based on second order conditions, $Q(\boldsymbol{\theta})$ is strictly convex in a ball \mathcal{N}_0 in the subspace \mathcal{B} centered at $\hat{\boldsymbol{\theta}}$. Thus, $\hat{\boldsymbol{\theta}}$ is a unique minimizer of $Q(\boldsymbol{\theta})$ in the neighborhood \mathcal{N}_0 .

Next, need to show that $\hat{\boldsymbol{\theta}}$ is a strict local minimizer of $Q(\boldsymbol{\theta})$ on the space $\mathbb{R}^{q+Np+T-1}$. Consider a sufficiently small ball \mathcal{N}_1 in $\mathbb{R}^{q+Np+T-1}$ centered at $\hat{\boldsymbol{\theta}}$ such that $\mathcal{N}_1 \cap \mathcal{B} \subset \mathcal{N}_0$. Need to show that $Q(\hat{\boldsymbol{\theta}}) < Q(\boldsymbol{\phi}_1)$ for any $\boldsymbol{\phi}_1 \in \mathcal{N}_1 \setminus \mathcal{N}_0$. Let $\boldsymbol{\phi}_2$ be the projection of $\boldsymbol{\phi}_1$ onto the subspace \mathcal{B} . Then, $\boldsymbol{\phi}_2 \in \mathcal{N}_0$, thus $Q(\hat{\boldsymbol{\theta}}) < Q(\boldsymbol{\phi}_2)$ for $\boldsymbol{\phi}_2 \neq \hat{\boldsymbol{\theta}}$ since $\hat{\boldsymbol{\theta}}$ is a local strict minimizer in \mathcal{N}_0 . Next, we will show that $Q(\boldsymbol{\phi}_2) < Q(\boldsymbol{\phi}_1)$. By the mean-value theorem,

$$Q(\boldsymbol{\phi}_1) - Q(\boldsymbol{\phi}_2) = [Q'(\boldsymbol{\phi}_0)]^\top (\boldsymbol{\phi}_1 - \boldsymbol{\phi}_2), \quad (34)$$

where $\boldsymbol{\phi}_0$ is a vector between $\boldsymbol{\phi}_1$ and $\boldsymbol{\phi}_2$, that is $\boldsymbol{\phi}_0 = \alpha_0 \boldsymbol{\phi}_1 + (1 - \alpha_0) \boldsymbol{\phi}_2$ and $\alpha_0 \in (0, 1)$. Based on the definition of $\boldsymbol{\phi}_1$ and $\boldsymbol{\phi}_2$, $\boldsymbol{\alpha}, \boldsymbol{\varsigma}_1, \boldsymbol{\varsigma}_{(1)}, \boldsymbol{\xi}_{(1)}$ are the elements of $\boldsymbol{\phi}_1$ in \mathcal{B} , then $\boldsymbol{\phi}_0 = (\boldsymbol{\alpha}, \boldsymbol{\varsigma}_1, \boldsymbol{\varsigma}_{(1)}, \boldsymbol{\xi}_{(1)}, \alpha_0 \boldsymbol{\varsigma}_{(2)}, \alpha_0 \boldsymbol{\xi}_{(2)})$. Thus, the right hand side of (34) can be expressed as

$$\begin{aligned} & - \frac{1}{NT} (\boldsymbol{y} - \boldsymbol{\mu}(\hat{\boldsymbol{\phi}}_0))^\top \mathbb{U}_2 \alpha_0 (\boldsymbol{\varsigma}_{(2)}^\top, \boldsymbol{\xi}_{(2)}^\top)^\top \\ & + \sum_{i \in \hat{\mathcal{N}}_N} \alpha_0 \|\boldsymbol{\varsigma}_i\| \mathcal{P}'_{\gamma_2}(\|\alpha_0 \boldsymbol{\varsigma}_i\|; \lambda_2) + \sum_{t \in \hat{\mathcal{N}}_T} \alpha_0 \mathcal{P}'_{\gamma_1}(|\alpha_0 \xi_t|; \lambda_1) |\xi_t|. \end{aligned} \quad (35)$$

Based on the conditions, there exists some $\delta > 0$ such that for any $\boldsymbol{\theta}$ in a ball centered at $\hat{\boldsymbol{\theta}}$ with radius δ ,

$$\begin{aligned}\left\| \frac{1}{NT} \mathbb{X}_{2(i)}^\top (\mathbf{y} - \boldsymbol{\mu}(\boldsymbol{\theta})) \right\|_\infty &< \mathcal{P}'_{\gamma_2}(\delta; \lambda_2) = \lambda_2 - \frac{\delta}{\gamma_2}, \\ \left\| \frac{1}{NT} \mathbb{M}_2^\top (\mathbf{y} - \boldsymbol{\mu}(\boldsymbol{\theta})) \right\|_\infty &< \mathcal{P}'_{\gamma_1}(\delta; \lambda_1) = \lambda_1 - \frac{\delta}{\gamma_1}.\end{aligned}$$

Consider the radius of the ball \mathcal{N}_1 to less than δ , then $|\xi_t| < \delta$, for $t \in \hat{\mathcal{N}}_T$ and $\|\mathbf{s}_i\| < \delta$, for $i \in \hat{\mathcal{N}}_N$, and above holds for any $\boldsymbol{\theta} \in \mathcal{N}_1$. And $\boldsymbol{\phi}_0 \in \mathcal{N}_1$, thus, (35) is strictly greater than the following

$$\begin{aligned}& -\alpha_0 \left(\lambda_2 - \frac{\delta}{\gamma_2} \right) \sum_{i \in \hat{\mathcal{N}}_N} \|\mathbf{s}_i\| - \alpha_0 \left(\lambda_1 - \frac{\delta}{\gamma_1} \right) \sum_{t \in \hat{\mathcal{N}}_T} |\xi_t| \\ & + \alpha_0 \left(\lambda_2 - \frac{\delta}{\gamma_2} \right) \sum_{i \in \hat{\mathcal{N}}_N} \|\mathbf{s}_i\| + \alpha_0 \left(\lambda_1 - \frac{\delta}{\gamma_1} \right) \sum_{t \in \hat{\mathcal{N}}_T} |\xi_t| = 0.\end{aligned}$$

Thus, $Q(\boldsymbol{\phi}_1) > Q(\boldsymbol{\phi}_2) > Q(\hat{\boldsymbol{\theta}})$. This completes the proof. \square

A.2 Lemma 2

Lemma 2. *Given the MST based on the weights in (16), consider any two locations i and i' in the same cluster. Under Condition (C4), there exists a path in the MST connecting i and i' such that all the locations on the path belong to the same cluster with probability approaching 1 as local sample size $T \rightarrow \infty$.*

Proof. For a given tree \mathcal{T} , we have $\|\hat{\boldsymbol{\theta}} - \boldsymbol{\theta}_{\mathcal{T},0}\| = O_P(\sqrt{s/N_0})$ from Theorem 1. Recall that \mathbf{s}_i represents difference between $\boldsymbol{\beta}_i - \boldsymbol{\beta}_{i'}$, $(i, i') \in \mathcal{E}$. And the $\boldsymbol{\beta} = (\tilde{\mathbf{H}}^{-1} \otimes \mathbf{I}_p) \boldsymbol{\varsigma}$, then $\|\hat{\boldsymbol{\beta}}_i - \boldsymbol{\beta}_i^0\| = O_P(\sqrt{s/T})$. Thus, we can calculate the difference between $\|\hat{\boldsymbol{\beta}}_i - \hat{\boldsymbol{\beta}}_{i'}\|$ in \mathcal{E}_0 . Recall the weights in (16),

$$w_{ii'} = \begin{cases} \|\hat{\boldsymbol{\beta}}_{\mathcal{T},i} - \hat{\boldsymbol{\beta}}_{\mathcal{T},i'}\| & (i, i') \in \mathcal{E}_0, \\ \infty & \text{otherwise.} \end{cases}$$

For $(i, i') \in \mathcal{E}_0$, we have

$$\begin{aligned}\|\hat{\boldsymbol{\beta}}_{\mathcal{T},i} - \hat{\boldsymbol{\beta}}_{\mathcal{T},i'}\| &\leq \|\hat{\boldsymbol{\beta}}_{\mathcal{T},i} - \boldsymbol{\beta}_i^0 - (\hat{\boldsymbol{\beta}}_{\mathcal{T},i'} - \boldsymbol{\beta}_{i'}^0) + \boldsymbol{\beta}_i^0 - \boldsymbol{\beta}_{i'}^0\| \\ &\leq \|\hat{\boldsymbol{\beta}}_{\mathcal{T},i} - \boldsymbol{\beta}_i^0\| + \|\hat{\boldsymbol{\beta}}_{\mathcal{T},i'} - \boldsymbol{\beta}_{i'}^0\| + \|\boldsymbol{\beta}_i^0 - \boldsymbol{\beta}_{i'}^0\|.\end{aligned}\tag{36}$$

If i and i' are in the same cluster, that means $\beta_i^0 = \beta_{i'}^0$, then (36) becomes

$$\|\hat{\beta}_{\mathcal{T},i} - \hat{\beta}_{\mathcal{T},i'}\| \leq \|\hat{\beta}_{\mathcal{T},i} - \beta_i^0\| + \|\hat{\beta}_{\mathcal{T},i'} - \beta_{i'}^0\| = O_P\left(\sqrt{s/T}\right).$$

This implies that $\|\hat{\beta}_{\mathcal{T},i} - \hat{\beta}_{\mathcal{T},i'}\|$ will converge to 0 with probability approaching 1 if i and i' are in the same cluster.

If i and i' are in different clusters, then (36) becomes,

$$\|\hat{\beta}_{\mathcal{T},i} - \hat{\beta}_{\mathcal{T},i'}\| = O_P\left(\sqrt{s/T}\right) + \|\beta_i^0 - \beta_{i'}^0\|.$$

This implies that $\|\hat{\beta}_{\mathcal{T},i} - \hat{\beta}_{\mathcal{T},i'}\|$ will converge to a constant depending on the cluster difference with probability approaching 1 if i and i' are in different clusters.

Then, by the same arguments of Zhang et al. (2022), the result in Lemma 2 holds. \square

Lemma 2 indicates that the graph will be separated into K subgraphs, corresponding to K clusters, by removing edges among clusters.

B Theorems

B.1 Proof of Theorem 1

In this proof, we use $\theta_{1,0}$ instead of $\theta_{\mathcal{T},1,0}$ for simplicity.

Proof. Without loss of generality, assume there are s_1 ξ_t 's are nonzero, they are $\xi_2, \dots, \xi_{s_1+1}$, and there are s_2 $\|\varsigma_i\|$ are nonzero, they are $\|\varsigma_2\|, \dots, \|\varsigma_{s_2+1}\|$. We will prove the result in two steps.

Step 1: Consistency in the s -dimensional subspace.

Consider the objective function $Q(\theta)$ on the s -dimensional subspace $\{\theta \in \mathbb{R}^{q+Np+T-1} : \theta_{\mathcal{S}_0^c} = \mathbf{0}\}$, where $\mathcal{S}_0 = \text{supp}(\theta_0)$, which is the nonzero set of the parameters, and \mathcal{S}_0^c is the complement. Then, the constrained objective function is

$$\bar{Q}(\delta) = \bar{l}(\delta) + \sum_{t=2}^{s_1+1} \mathcal{P}_{\gamma_1}(|\xi_t|; \lambda_1) + \sum_{i=2}^{s_2+1} \mathcal{P}_{\gamma_2}(\|\varsigma_i\|, \lambda_2),$$

where $\bar{l}(\delta) = \frac{1}{NT} \left(-\mathbf{y}^T \mathbb{U}_1 \delta + \mathbf{1}^T \boldsymbol{\mu}(\delta)\right) = \frac{1}{NT} \left(-\mathbf{y}^T \left(\mathbf{Z}\boldsymbol{\alpha} + \mathbb{X}_1 \varsigma_{(1)} + \mathbb{M}_1 \boldsymbol{\xi}_{(1)}\right) + \mathbf{1}^T \boldsymbol{\mu}(\delta)\right)$, here $\boldsymbol{\mu}(\delta) = (n_{it} \exp(b_{it}))_{1 \leq i \leq N, 1 \leq t \leq T}$, with $\mathbf{b} = \mathbb{U}_1 \delta$. We now show that there exists

a strict local minimizer of $\hat{\boldsymbol{\theta}}_1$ of $\bar{Q}(\boldsymbol{\delta})$ such that $\|\hat{\boldsymbol{\theta}}_1 - \boldsymbol{\theta}_{1,0}\| = O_P(\sqrt{s/N_0})$, where $s = s_1 + s_2p$ and $N_0 = NT$.

Define an event

$$H_1 = \left\{ \bar{Q}(\boldsymbol{\theta}_{1,0}) < \min_{\boldsymbol{\delta} \in \partial \mathcal{N}_C} \bar{Q}(\boldsymbol{\delta}) \right\},$$

where $\partial \mathcal{N}_C$ denotes the boundary of the closet set $\mathcal{N}_C = \{\|\boldsymbol{\delta} - \boldsymbol{\theta}_{1,0}\| \leq C\sqrt{s/N_0}\}$ and $C \in (0, \infty)$. On event H_1 , there exists a local minimizer $\hat{\boldsymbol{\theta}}_1$ of $\bar{Q}(\boldsymbol{\delta})$ in \mathcal{N}_C . We need to show that $P(H_1)$ is close to 1 as $T \rightarrow \infty$ when C is large.

Let T be sufficiently large such that $\sqrt{s/N_0}C \leq d$, δ_{ξ_t} is the element in $\boldsymbol{\delta}$ in \mathcal{N}_C corresponds to ξ_t , and $\boldsymbol{\delta}_{\boldsymbol{\varsigma}_i}$ is the element in $\boldsymbol{\delta}$ in \mathcal{N}_C corresponds to $\boldsymbol{\varsigma}_i$. By Taylor expansion, for $\boldsymbol{\delta} \in \partial \mathcal{N}_C$,

$$\bar{Q}(\boldsymbol{\delta}) - \bar{Q}(\boldsymbol{\theta}_{1,0}) = (\boldsymbol{\delta} - \boldsymbol{\theta}_{1,0})^\top \boldsymbol{v} + \frac{1}{2} (\boldsymbol{\delta} - \boldsymbol{\theta}_{1,0})^\top \boldsymbol{D} (\boldsymbol{\delta} - \boldsymbol{\theta}_{1,0}),$$

where \boldsymbol{v} is the first order derivative of $\bar{Q}(\boldsymbol{\delta})$ evaluated at $\boldsymbol{\theta}_{1,0}$, and \boldsymbol{D} is the second order derivative of $\bar{Q}(\boldsymbol{\delta})$ evaluated at $\boldsymbol{\theta}_1^*$ with $\boldsymbol{\theta}_1^* = \alpha_1 \boldsymbol{\delta} + (1 - \alpha_1) \boldsymbol{\theta}_{1,0}$ and $\alpha_1 \in (0, 1)$. We have

$$\boldsymbol{v} = -\frac{1}{NT} \mathbb{U}_1^\top (\boldsymbol{y} - \boldsymbol{\mu}(\boldsymbol{\theta}_{1,0})) + \left(\mathbf{0}, \frac{\boldsymbol{\varsigma}_i}{\|\boldsymbol{\varsigma}_i\|} \mathcal{P}'_{\gamma_2}(\|\boldsymbol{\varsigma}_i\|; \lambda_2), i = 2, \dots, s_2 + 1, \mathcal{P}'_{\gamma_1}(\xi_t; \lambda_1); t = 2, \dots, s_1 + 1 \right),$$

$$\boldsymbol{D} = \frac{1}{NT} \mathbb{U}_1^\top \boldsymbol{\Sigma}(\boldsymbol{\theta}_1^*) \mathbb{U}_1 + \text{diag} \left(\mathbf{0}, \left[\frac{\boldsymbol{\varsigma}_i^*}{\|\boldsymbol{\varsigma}_i^*\|} \mathcal{P}'_{\gamma_2}(\|\boldsymbol{\varsigma}_i^*\|; \lambda_2) \right]', i = 2, \dots, s_2 + 1, \mathcal{P}''_{\gamma_1}(\xi_t^*; \lambda_1); t = 2, \dots, s_1 + 1 \right)$$

Recall that $\boldsymbol{\delta} \in \partial \mathcal{N}_C$, thus $\|\boldsymbol{\delta} - \boldsymbol{\theta}_{1,0}\| = C\sqrt{s/N_0}$. Since $\boldsymbol{\theta}_1^* = \alpha_1 \boldsymbol{\delta} + (1 - \alpha_1) \boldsymbol{\theta}_{1,0}$, we have $\|\boldsymbol{\theta}_1^* - \boldsymbol{\theta}_{1,0}\| = \|\alpha_1 (\boldsymbol{\delta} - \boldsymbol{\theta}_{1,0})\| = \alpha_1 \|\boldsymbol{\delta} - \boldsymbol{\theta}_{1,0}\|$, thus $\boldsymbol{\theta}_1^* \in \mathcal{N}_0$. When T is sufficiently large, since $d \gg \sqrt{s/N_0}$, then, $|\xi_t^*| \geq |\xi_t| - C\sqrt{s/N_0} \geq d$, and $\|\boldsymbol{\varsigma}_i^*\| \geq \|\boldsymbol{\varsigma}_i\| - C\sqrt{s/N_0} \geq d$ based on Condition (C3). Based on the definition of MCP and assumption that $d \gg \max(\lambda_1, \lambda_2)$, we have $d \gg \max(\gamma_1 \lambda_1, \gamma_2 \lambda_2)$, thus $\mathcal{P}''_{\gamma_1}(\xi_t^*; \lambda_1) = 0$ and $\mathcal{P}''_{\gamma_2}(\|\boldsymbol{\varsigma}_i^*\|; \lambda_2) = 0$ and $\mathcal{P}'_{\gamma_2}(\|\boldsymbol{\varsigma}_i^*\|; \lambda_2) = 0$. Then, we have the following result:

$$\left[\frac{\boldsymbol{\varsigma}_i^*}{\|\boldsymbol{\varsigma}_i^*\|} \mathcal{P}'_{\gamma_2}(\|\boldsymbol{\varsigma}_i^*\|; \lambda_2) \right]' = \frac{\boldsymbol{\varsigma}_i^* \boldsymbol{\varsigma}_i^{*\top}}{\|\boldsymbol{\varsigma}_i^*\|^2} \mathcal{P}''_{\gamma_2}(\|\boldsymbol{\varsigma}_i^*\|; \lambda_2) + \frac{\mathcal{P}'_{\gamma_2}(\|\boldsymbol{\varsigma}_i^*\|; \lambda_2)}{\|\boldsymbol{\varsigma}_i^*\|} \boldsymbol{I}_p - \frac{\boldsymbol{\varsigma}_i^* \boldsymbol{\varsigma}_i^{*\top} \mathcal{P}'_{\gamma_2}(\|\boldsymbol{\varsigma}_i^*\|; \lambda_2)}{\|\boldsymbol{\varsigma}_i^*\|^3} = \mathbf{0}.$$

Thus, $\lambda_{\min}(\boldsymbol{D}) = \lambda_{\min}(\frac{1}{NT} \mathbb{U}_1^\top \boldsymbol{\Sigma}(\boldsymbol{\theta}_1^*) \mathbb{U}_1) \geq c_1 M_1$. Also within \mathcal{N}_C , we have $|\delta_{\xi_t}| \geq |\xi_t| - C\sqrt{s/N_0} \geq d$, and $\|\boldsymbol{\delta}_{\boldsymbol{\varsigma}_i}\| \geq \|\boldsymbol{\varsigma}_i\| - C\sqrt{s/N_0} \geq d$, $\|\boldsymbol{\varsigma}_i\| \geq d$ and $|\xi_t| \geq d$, thus $\mathcal{P}'_{\gamma_2}(\|\boldsymbol{\varsigma}_i\|; \lambda_2) = 0$ and $\mathcal{P}'_{\gamma_1}(\xi_t; \lambda_1) = 0$ based on $d \gg \max(\gamma_1 \lambda_1, \gamma_2 \lambda_2)$.

Thus, we have

$$\begin{aligned}
& \min_{\boldsymbol{\delta} \in \partial \mathcal{N}_C} \bar{Q}(\boldsymbol{\delta}) - \bar{Q}(\boldsymbol{\theta}_{1,0}) \\
& \geq - \left\| \frac{1}{NT} \mathbb{U}_1^\top (\mathbf{y} - \boldsymbol{\mu}(\boldsymbol{\theta}_{1,0})) \right\| \|\boldsymbol{\delta} - \boldsymbol{\theta}_{1,0}\| + c_1 M_1 \frac{1}{2} \|\boldsymbol{\delta} - \boldsymbol{\theta}_{1,0}\|^2 \\
& = - C \sqrt{s/N_0} \left\| \frac{1}{NT} \mathbb{U}_1^\top (\mathbf{y} - \boldsymbol{\mu}(\boldsymbol{\theta}_{1,0})) \right\| + c_1 M_1 \frac{1}{2} \|\boldsymbol{\delta} - \boldsymbol{\theta}_{1,0}\|^2 \\
& = - C \sqrt{s/N_0} \left[\left\| \frac{1}{NT} \mathbb{U}_1^\top (\mathbf{y} - \boldsymbol{\mu}(\boldsymbol{\theta}_{1,0})) \right\| - \frac{c_1 M_1 C \sqrt{s/N_0}}{2} \right].
\end{aligned}$$

Based on Markov's inequality,

$$\begin{aligned}
P(H_1) & \geq P \left[\left\| \frac{1}{NT} \mathbb{U}_1^\top (\mathbf{y} - \boldsymbol{\mu}(\boldsymbol{\theta}_{1,0})) \right\|^2 < \frac{c_1^2 M_1^2 C^2 s}{4N_0} \right] \\
& \geq 1 - \frac{4N_0 E \left\| \frac{1}{NT} \mathbb{U}_1^\top (\mathbf{y} - \boldsymbol{\mu}(\boldsymbol{\theta}_{1,0})) \right\|^2}{c_1^2 M_1^2 C^2 s}.
\end{aligned}$$

We know that $E(\mathbf{y}) = \boldsymbol{\mu}(\boldsymbol{\theta}_{1,0})$, $Var(\mathbf{y}) = \boldsymbol{\Sigma}(\boldsymbol{\theta}_{1,0}) = \text{diag}(\boldsymbol{\mu}(\boldsymbol{\theta}_{1,0}))$, and $E \left\| \frac{1}{NT} \mathbb{U}_1^\top (\mathbf{y} - \boldsymbol{\mu}(\boldsymbol{\theta}_{1,0})) \right\|^2 = \frac{1}{N_0^2} \text{tr}(\mathbb{U}_1^\top \boldsymbol{\Sigma}(\boldsymbol{\theta}_0) \mathbb{U}_1) \leq \frac{sc_2 M_2}{N_0}$. Thus

$$P(H_1) \geq 1 - \frac{4N_0 s c_2 M_2}{N_0 c_1^2 M_1^2 C^2 s} = 1 - \frac{4c_2 M_2}{c_1^2 M_1^2} \frac{1}{C^2}.$$

As $C \rightarrow \infty$, $P(H_1) \rightarrow 1$. This proves that $\|\hat{\boldsymbol{\theta}}_1 - \boldsymbol{\theta}_{1,0}\| = O_P(\sqrt{s/N_0})$.

Step 2: Sparsity.

Let $\hat{\boldsymbol{\theta}} = (\hat{\boldsymbol{\theta}}_1, \hat{\boldsymbol{\theta}}_2)$, where $\hat{\boldsymbol{\theta}}_1 \in \mathcal{N}_C \subset \mathcal{N}_0$ is a strict local minimizer of $\bar{Q}(\boldsymbol{\delta})$ and $\hat{\boldsymbol{\theta}}_2 = \mathbf{0}$. We need to show that $\hat{\boldsymbol{\theta}}$ is a strict local minimizer of $Q(\boldsymbol{\theta})$.

Let $\boldsymbol{\varphi} = \mathbb{U}^\top (\mathbf{y} - \boldsymbol{\mu}(\boldsymbol{\theta}_0))$, and consider the event

$$\mathcal{E}_1 = \left\{ \max_{i=s_2+2, \dots, N} \|\mathbb{X}_{2(i)}(\mathbf{y} - \boldsymbol{\mu}(\boldsymbol{\theta}_0))\| \leq u\sqrt{N_0}; \quad \max_{t=s_1+2, \dots, T} |\mathbb{M}_{2(t)}(\mathbf{y} - \boldsymbol{\mu}(\boldsymbol{\theta}_0))| \leq u\sqrt{N_0} \right\}.$$

Based on conditions (C1) and (C2), conditions in (27), (28), (29) and (30) are satisfied. (21), (22), (23) and (24) are satisfied based on the definition of $\hat{\boldsymbol{\theta}}_1$. Thus, it suffices to check conditions (25) and (26).

From Fan and Lv (2011), we have

$$P(|\mathbf{a}^\top (\mathbf{y} - \boldsymbol{\mu}(\boldsymbol{\theta}_0))| > \|\mathbf{a}\|_{2\epsilon}) \leq 2e^{-c_3 \epsilon^2}, \tag{37}$$

where c_3 is a positive constant. Let $\mathbb{M}_{(j)}$ be the j th column of \mathbb{M} and satisfy $\max_j \|\mathbb{M}_{(j)}\| = \sqrt{(T-1)N}$ based on the construction of \mathbb{M} . Let $\mathbb{X}_{2(ij)}$ be the j th column of $\mathbb{X}_{2(i)}$ and $\max_{i,j} \|\mathbb{X}_{2(ij)}\| = O(\sqrt{N_0})$ based on condition (C1). It follows from Bonferroni's inequality, we have

$$P(\mathcal{E}_1) \geq 1 - \sum_{i=s_2+2}^N \sum_{j=1}^p P\left(\|\mathbb{X}_{2(ij)}^\top (\mathbf{y} - \boldsymbol{\mu}(\boldsymbol{\theta}_0))\| > u\sqrt{N_0}\right) - \sum_{t=s_1+2}^T P\left(|\mathbb{M}_{2(t-1)}^\top (\mathbf{y} - \boldsymbol{\mu}(\boldsymbol{\theta}_0))| > u\sqrt{N_0}\right)$$

where $u \gg \sqrt{\log N_0}$ and $uN_0^{-1/2} = o(1)$.

From (37), we have

$$\begin{aligned} P\left(\|\mathbb{X}_{2(ij)}^\top (\mathbf{y} - \boldsymbol{\mu}(\boldsymbol{\theta}_0))\| > u\sqrt{N_0}\right) &= P\left(\|\mathbb{X}_{2(ij)}^\top (\mathbf{y} - \boldsymbol{\mu}(\boldsymbol{\theta}_0))\| > \|\mathbb{X}_{2(ij)}^\top\| \frac{u\sqrt{N_0}}{\|\mathbb{X}_{2(ij)}\|}\right) \\ &\leq P\left(\|\mathbb{X}_{2(ij)}^\top (\mathbf{y} - \boldsymbol{\mu}(\boldsymbol{\theta}_0))\| > \|\mathbb{X}_{2(ij)}^\top\| \frac{u\sqrt{N_0}}{\max_{i,j} \|\mathbb{X}_{2(ij)}\|}\right) \\ &\leq 2e^{-c_3 u^2} \end{aligned}$$

and

$$\begin{aligned} P\left(|\mathbb{M}_{2(t-1)}^\top (\mathbf{y} - \boldsymbol{\mu}(\boldsymbol{\theta}_0))| > u\sqrt{N_0}\right) &= P\left(|\mathbb{M}_{2(t-1)}^\top (\mathbf{y} - \boldsymbol{\mu}(\boldsymbol{\theta}_0))| > \|\mathbb{M}_{2(t-1)}^\top\| \frac{u\sqrt{N_0}}{\|\mathbb{M}_{2(t-1)}\|}\right) \\ &\leq P\left(|\mathbb{M}_{2(t-1)}^\top (\mathbf{y} - \boldsymbol{\mu}(\boldsymbol{\theta}_0))| > \|\mathbb{M}_{2(t-1)}^\top\| \frac{u\sqrt{N_0}}{\max_j \|\mathbb{M}_{2(t-1)}\|}\right) \\ &\leq P\left(|\mathbb{M}_{2(t-1)}^\top (\mathbf{y} - \boldsymbol{\mu}(\boldsymbol{\theta}_0))| > \|\mathbb{M}_{2(t-1)}^\top\| \frac{u\sqrt{N_0}}{\sqrt{N_0}}\right) \\ &\leq 2e^{-c_3 u^2}. \end{aligned}$$

Thus

$$P(\mathcal{E}_1) \geq 1 - ((N - s_2 - 1)p + T - s_1 - 1)e^{-c_3 u^2} \geq 1 - \frac{Np + T}{e^{c_3 u^2}} \geq 1 - \frac{1}{e^{c_3 u^2 - \log N_0}} \rightarrow 1.$$

Under event \mathcal{E}_1 , now consider the following in (25),

$$\left\| \frac{1}{NT} \mathbb{X}_{2(i)}^\top (\mathbf{y} - \boldsymbol{\mu}(\hat{\boldsymbol{\theta}})) \right\| \leq \left\| \frac{1}{NT} \mathbb{X}_{2(i)}^\top (\mathbf{y} - \boldsymbol{\mu}(\boldsymbol{\theta}_0)) \right\| + \left\| \frac{1}{NT} \mathbb{X}_{2(i)}^\top (\boldsymbol{\mu}(\boldsymbol{\theta}_0) - \boldsymbol{\mu}(\hat{\boldsymbol{\theta}})) \right\|.$$

The first part is bounded by $\frac{u\sqrt{N_0}}{N_0} = uN_0^{-1/2} \ll \lambda_2$ by condition (C3).

Next, consider the second part $\frac{1}{NT} \mathbb{X}_{2(i)}^\top (\boldsymbol{\mu}(\hat{\boldsymbol{\theta}}) - \boldsymbol{\mu}(\boldsymbol{\theta}_0))$. According to the Taylor expansion,

$$\begin{aligned} \mathbb{X}_{2(i)}^\top (\boldsymbol{\mu}(\hat{\boldsymbol{\theta}}) - \boldsymbol{\mu}(\boldsymbol{\theta}_0)) &= \mathbb{X}_{2(i)}^\top (\boldsymbol{\mu}(\hat{\boldsymbol{\theta}}_1) - \boldsymbol{\mu}(\boldsymbol{\theta}_{1,0})) \\ &= \mathbb{X}_{2(i)}^\top \boldsymbol{\Sigma}(\boldsymbol{\theta}_{1,0}) \mathbb{X}_1 (\hat{\boldsymbol{\theta}}_1 - \boldsymbol{\theta}_{1,0}) + \boldsymbol{w}, \end{aligned}$$

where $w_j = \frac{1}{2} (\hat{\boldsymbol{\theta}}_1 - \boldsymbol{\theta}_{1,0})^\top \nabla_j (\hat{\boldsymbol{\theta}}_1 - \boldsymbol{\theta}_{1,0})$, $\nabla_j = \mathbb{X}_1^\top \text{diag}(x_{2(ij)} \boldsymbol{\mu}(\boldsymbol{\theta}_1^*)) \mathbb{X}_1$ and $\boldsymbol{\theta}_1^*$ is a vector lying on the line segment jointing $\hat{\boldsymbol{\theta}}_1$ and $\boldsymbol{\theta}_{1,0}$. Since all x are bounded, then $\|\boldsymbol{w}\|_\infty \leq \frac{1}{2} M_x N_0 \lambda_{\max} \left[\frac{1}{NT} \mathbb{X}_1^\top \mathbb{X}_1 \right] \|\hat{\boldsymbol{\theta}}_1 - \boldsymbol{\theta}_{1,0}\|^2 = O(N_0) \|\hat{\boldsymbol{\theta}}_1 - \boldsymbol{\theta}_{1,0}\|^2$, where M_x is a positive constant. Similarly,

$$\|\mathbb{X}_{2(i)}^\top \boldsymbol{\Sigma}(\boldsymbol{\theta}_{1,0}) \mathbb{X}_1 (\hat{\boldsymbol{\theta}}_1 - \boldsymbol{\theta}_{1,0})\| = O(N_0) \|\hat{\boldsymbol{\theta}}_1 - \boldsymbol{\theta}_{1,0}\|.$$

Thus,

$$\left\| \frac{1}{NT} \mathbb{X}_{2(i)}^\top (\boldsymbol{y} - \boldsymbol{\mu}(\hat{\boldsymbol{\theta}})) \right\| = o(\lambda_2) + O(\|\hat{\boldsymbol{\theta}}_1 - \boldsymbol{\theta}_{1,0}\| + \|\hat{\boldsymbol{\theta}}_1 - \boldsymbol{\theta}_{1,0}\|^2).$$

Since $\lambda_2 \gg \sqrt{s/N_0}$, thus $\|\hat{\boldsymbol{\theta}}_1 - \boldsymbol{\theta}_{1,0}\| + \|\hat{\boldsymbol{\theta}}_1 - \boldsymbol{\theta}_{1,0}\|^2 = o(\lambda_2)$. Thus $\left\| \frac{1}{NT} \mathbb{X}_{2(i)}^\top (\boldsymbol{y} - \boldsymbol{\mu}(\hat{\boldsymbol{\theta}})) \right\| = o(\lambda_2)$. The condition in (25) holds.

By similar arguments, we can have (26) hold. This completes the proof. \square

B.2 Proof of Theorem 2

Proof. Let \mathcal{W} be an event that for a given MST, \mathcal{T} , for any two locations i and i' in the same cluster, there exists a path in the MST connecting i and i' such that all the locations on the path belong to the same cluster. This means that in event \mathcal{W} , when the nonzero values of $\boldsymbol{\varsigma}_i$ are identified, which means the nonzero edges are identified. This implies that the true cluster structure of $\boldsymbol{\beta}$ can be recovered.

Let $\hat{\boldsymbol{\theta}}_{\mathcal{W}}$ be the estimator when \mathcal{W} occurs, and $\hat{\boldsymbol{\theta}}_{\mathcal{W}^c}$ be the estimator when \mathcal{W} does not occur, then $\hat{\boldsymbol{\theta}} = \hat{\boldsymbol{\theta}}_{\mathcal{W}} I\{\mathcal{W}\} + \hat{\boldsymbol{\theta}}_{\mathcal{W}^c} I\{\mathcal{W}^c\}$. Then, we have

$$\sqrt{N_0/s} \|\hat{\boldsymbol{\theta}} - \boldsymbol{\theta}_0\| = \sqrt{N_0/s} (\hat{\boldsymbol{\theta}}_{\mathcal{W}} - \boldsymbol{\theta}_0) I\{\mathcal{W}\} + \sqrt{N_0/s} (\hat{\boldsymbol{\theta}}_{\mathcal{W}^c} - \boldsymbol{\theta}_0) I\{\mathcal{W}^c\}.$$

From Theorem 1, we have that $\sqrt{N_0/s} (\hat{\boldsymbol{\theta}}_{\mathcal{W}} - \boldsymbol{\theta}_0) = O_P(1)$ and $\sqrt{N_0/s} (\hat{\boldsymbol{\theta}}_{\mathcal{W}^c} - \boldsymbol{\theta}_0) = O_P(1)$. Also $P(\mathcal{W}) \rightarrow 1$ and $P(\mathcal{W}^c) \rightarrow 0$ from Lemma 2. Thus, $\sqrt{N_0/s} \|\hat{\boldsymbol{\theta}} - \boldsymbol{\theta}_0\|$ converges to the same distribution of $\sqrt{N_0/s} (\hat{\boldsymbol{\theta}}_{\mathcal{W}} - \boldsymbol{\theta}_0)$.

Besides this, we also have the following results.

$$\begin{aligned} P(\hat{\mathcal{S}}_N^* = \mathcal{S}_N^*) &= P(\hat{\mathcal{S}}_N^* = \mathcal{S}_N^* | \mathcal{W}) P(\mathcal{W}) + P(\hat{\mathcal{S}}_N^* = \mathcal{S}_N | \mathcal{W}^c) P(\mathcal{W}^c) \\ &\rightarrow 1, \end{aligned}$$

since $P(\mathcal{W}) \rightarrow 1$ and $P(\mathcal{W}^c) \rightarrow 0$. We can also have $P(\hat{\mathcal{S}}_T^* = \mathcal{S}_T) \rightarrow 1$ by the same arguments. \square

References

- Allevius, B. (2018). scanstatistics: Space-time anomaly detection using scan statistics. *Journal of Open Source Software*, 3(25):515.
- Altieri, L., Scott, E. M., Cocchi, D., and Illian, J. B. (2015). A changepoint analysis of spatio-temporal point processes. *Spatial Statistics*, 14:197–207.
- Amin, R. W., Fritsch, B. A., and Retzliff, J. E. (2019). Spatial clusters of breast cancer mortality and incidence in the contiguous USA: 2000–2014. *Journal of General Internal Medicine*, 34:412–419.
- Anderson, C., Lee, D., and Dean, N. (2017). Spatial clustering of average risks and risk trends in Bayesian disease mapping. *Biometrical Journal*, 59(1):41–56.
- Ansari, M. Y., Ahmad, A., Khan, S. S., Bhushan, G., and Mainuddin (2020). Spatiotemporal clustering: a review. *Artificial Intelligence Review*, 53:2381–2423.
- Assunção, R., Tavares, A., Correa, T., and Kulldorff, M. (2007). Space-time cluster identification in point processes. *Canadian Journal of Statistics*, 35(1):9–25.
- Besag, J. and Higdon, D. (1999). Bayesian analysis of agricultural field experiments. *Journal of the Royal Statistical Society Series B: Statistical Methodology*, 61(4):691–746.
- Chan, N. H., Yau, C. Y., and Zhang, R.-M. (2014). Group LASSO for structural break time series. *Journal of the American Statistical Association*, 109(506):590–599.
- Chernyavskiy, P., Kennerley, V. M., Jemal, A., Little, M. P., and Rosenberg, P. S. (2019). Heterogeneity of colon and rectum cancer incidence across 612 SEER counties, 2000–2014. *International Journal of Cancer*, 144(8):1786–1795.

- Cho, H. (2016). Change-point detection in panel data via double CUSUM statistic. *Electronic Journal of Statistics*, 10:2000–2038.
- Cho, H. and Fryzlewicz, P. (2015). Multiple-change-point detection for high dimensional time series via sparsified binary segmentation. *Journal of the Royal Statistical Society Series B: Statistical Methodology*, 77(2):475–507.
- Daly, M. C. and Paquette, I. M. (2019). Surveillance, epidemiology, and end results (seer) and seer-medicare databases: use in clinical research for improving colorectal cancer outcomes. *Clinics in colon and rectal surgery*, 32(01):061–068.
- Duggan, M. A., Anderson, W. F., Altekruse, S., Penberthy, L., and Sherman, M. E. (2016). The surveillance, epidemiology and end results (seer) program and pathology: towards strengthening the critical relationship. *The American journal of surgical pathology*, 40(12):e94.
- Fan, J. and Lv, J. (2011). Nonconcave penalized likelihood with NP-dimensionality. *IEEE Transactions on Information Theory*, 57(8):5467–5484.
- Frévent, C., Ahmed, M.-S., Dabo-Niang, S., and Genin, M. (2023). Investigating spatial scan statistics for multivariate functional data. *Journal of the Royal Statistical Society Series C: Applied Statistics*, 72(2):450–475.
- Frévent, C., Ahmed, M.-S., Marbac, M., and Genin, M. (2021). Detecting spatial clusters in functional data: New scan statistic approaches. *Spatial Statistics*, 46:100550.
- Frévent, C., Ahmed, M.-S., Soula, J., Smida, Z., Cucala, L., Dabo-Niang, S., and Genin, M. (2022). The R package HDSpatialScan for the detection of clusters of multivariate and functional data using spatial scan statistics. *R Journal*, 14(3).
- Geng, L. and Hu, G. (2022). Bayesian spatial homogeneity pursuit for survival data with an application to the SEER respiratory cancer data. *Biometrics*, 78(2):536–547.
- Gong, P., Zhang, C., Lu, Z., Huang, J., and Ye, J. (2013). A general iterative shrinkage and thresholding algorithm for non-convex regularized optimization problems. In *international conference on machine learning*, pages 37–45. PMLR.
- Gromenko, O., Kokoszka, P., and Reimherr, M. (2017). Detection of change in the spatiotemporal mean function. *Journal of the Royal Statistical Society Series B: Statistical Methodology*, 79(1):29–50.

- Güemes, A., Ray, S., Aboumerhi, K., Desjardins, M. R., Kvit, A., Corrigan, A. E., Fries, B., Shields, T., Stevens, R. D., Curriero, F. C., et al. (2021). A syndromic surveillance tool to detect anomalous clusters of COVID-19 symptoms in the United States. *Scientific reports*, 11(1):4660.
- Guha, A., Fradley, M. G., Dent, S. F., Weintraub, N. L., Lustberg, M. B., Alonso, A., and Addison, D. (2022). Incidence, risk factors, and mortality of atrial fibrillation in breast cancer: a seer-medicare analysis. *European heart journal*, 43(4):300–312.
- Gusev, A. (2008). Temporal structure of the global sequence of volcanic eruptions: Order clustering and intermittent discharge rate. *Physics of the Earth and planetary interiors*, 166(3-4):203–218.
- Harchaoui, Z. and Lévy-Leduc, C. (2010). Multiple change-point estimation with a total variation penalty. *Journal of the American Statistical Association*, 105(492):1480–1493.
- Hardisty, F. and Klippel, A. (2010). Analysing spatio-temporal autocorrelation with LISTA-Viz. *International Journal of Geographical Information Science*, 24(10):1515–1526.
- Hubert, L. and Arabie, P. (1985). Comparing partitions. *Journal of classification*, 2(1):193–218.
- Jung, I. (2009). A generalized linear models approach to spatial scan statistics for covariate adjustment. *Statistics in medicine*, 28(7):1131–1143.
- Kamenetsky, M. E., Lee, J., Zhu, J., and Gangnon, R. E. (2022). Regularized spatial and spatio-temporal cluster detection. *Spatial and Spatio-temporal Epidemiology*, 41:100462.
- Kulldorff, M. (2001). Prospective time periodic geographical disease surveillance using a scan statistic. *Journal of the Royal Statistical Society: Series A (Statistics in Society)*, 164(1):61–72.
- Kulldorff, M., Heffernan, R., Hartman, J., Assunção, R., and Mostashari, F. (2005). A space-time permutation scan statistic for disease outbreak detection. *PLoS medicine*, 2(3):e59.
- Law, J., Quick, M., and Chan, P. (2014). Bayesian spatio-temporal modeling for analysing local patterns of crime over time at the small-area level. *Journal of quantitative criminology*, 30:57–78.

- Lee, D.-T. and Schachter, B. J. (1980). Two algorithms for constructing a Delaunay triangulation. *International Journal of Computer & Information Sciences*, 9(3):219–242.
- Lee, J., Gangnon, R. E., and Zhu, J. (2017). Cluster detection of spatial regression coefficients. *Statistics in medicine*, 36(7):1118–1133.
- Lee, J., Kamenetsky, M. E., Gangnon, R. E., and Zhu, J. (2021). Clustered spatio-temporal varying coefficient regression model. *Statistics in medicine*, 40(2):465–480.
- Lee, J., Sun, Y., and Chang, H. H. (2020). Spatial cluster detection of regression coefficients in a mixed-effects model. *Environmetrics*, 31(2):e2578.
- Li, F. and Sang, H. (2019). Spatial homogeneity pursuit of regression coefficients for large datasets. *Journal of the American Statistical Association*, 114(527):1050–1062.
- Li, Q. and Wang, L. (2020). Robust change point detection method via adaptive LAD-LASSO. *Statistical Papers*, 61:109–121.
- Lin, F., Tang, Y., Zhu, H., and Zhu, Z. (2022). Spatially clustered varying coefficient model. *Journal of Multivariate Analysis*, 192:105023.
- Liu, L. and Lin, L. (2019). Subgroup analysis for heterogeneous additive partially linear models and its application to car sales data. *Computational Statistics & Data Analysis*, 138:239–259.
- Loh, P.-L. and Wainwright, M. J. (2015). Regularized m-estimators with nonconvexity: Statistical and algorithmic theory for local optima. *Journal of Machine Learning Research*, 16(1):559–616.
- Ma, S., Huang, J., Zhang, Z., and Liu, M. (2020). Exploration of heterogeneous treatment effects via concave fusion. *The international journal of biostatistics*, 16(1).
- Mohammadi, A., Bergquist, R., Fathi, G., Pishgar, E., de Melo, S. N., Sharifi, A., and Kiani, B. (2022). Homicide rates are spatially associated with built environment and socio-economic factors: A study in the neighbourhoods of Toronto, Canada. *BMC public health*, 22(1):1–19.

- Napier, G., Lee, D., Robertson, C., and Lawson, A. (2019). A bayesian space–time model for clustering areal units based on their disease trends. *Biostatistics*, 20(4):681–697.
- Paradinas, I., Conesa, D., López-Quílez, A., and Bellido, J. M. (2017). Spatio-temporal model structures with shared components for semi-continuous species distribution modelling. *Spatial Statistics*, 22:434–450.
- Rogerson, P. A. (2001). Monitoring point patterns for the development of space–time clusters. *Journal of the Royal Statistical Society: Series A (Statistics in Society)*, 164(1):87–96.
- Sasaki, Y. (2007). The truth of the F-measure. *Teach tutor mater*, 1(5):1–5.
- Schmid, V. and Held, L. (2004). Bayesian extrapolation of space–time trends in cancer registry data. *Biometrics*, 60(4):1034–1042.
- SEER (2023). Surveillance, epidemiology, and end results (SEER) program (www.seer.cancer.gov) SEER*Stat Database: Incidence - SEER Research Data, 8 Registries, Nov 2021 Sub (1975-2020) - Linked To County Attributes - Time Dependent (1990-2020) Income/Rurality, 1969-2020 Counties, National Cancer Institute, DCCPS, Surveillance Research Program, released April 2023, based on the November 2022 submission.
- Siljander, M., Uusitalo, R., Pellikka, P., Isosomppi, S., and Vapalahti, O. (2022). Spatiotemporal clustering patterns and sociodemographic determinants of COVID-19 (SARS-CoV-2) infections in helsinki, finland. *Spatial and spatio-temporal epidemiology*, 41:100493.
- Smida, Z., Cucala, L., Gannoun, A., and Durif, G. (2022). A wilcoxon-mann-whitney spatial scan statistic for functional data. *Computational Statistics & Data Analysis*, 167:107378.
- Tolwin, Y., Gillis, R., and Peled, N. (2020). Gender and lung cancer—seer-based analysis. *Annals of Epidemiology*, 46:14–19.
- Tzala, E. and Best, N. (2008). Bayesian latent variable modelling of multivariate spatio-temporal variation in cancer mortality. *Statistical methods in medical research*, 17(1):97–118.

- Wang, T. and Samworth, R. J. (2018). High dimensional change point estimation via sparse projection. *Journal of the Royal Statistical Society Series B: Statistical Methodology*, 80(1):57–83.
- Wang, X. (2023). Clustering of longitudinal curves via a penalized method and EM algorithm. *Computational Statistics*, pages 1–28.
- Wang, X., Zhang, X., and Zhu, Z. (2023a). Clustered coefficient regression models for Poisson process with an application to seasonal warranty claim data. *Technometrics*, 0(0):1–10.
- Wang, X., Zhu, Z., and Zhang, H. H. (2023b). Spatial heterogeneity automatic detection and estimation. *Computational Statistics & Data Analysis*, 180:107667.
- Xie, Y. and Siegmund, D. (2012). Spectrum opportunity detection with weak and correlated signals. In *2012 Conference Record of the Forty Sixth Asilomar Conference on Signals, Systems and Computers (ASILOMAR)*, pages 128–132. IEEE.
- Zhang, C.-H. (2010). Nearly unbiased variable selection under minimax concave penalty. *The Annals of statistics*, 38(2):894–942.
- Zhang, X., Liu, J., and Zhu, Z. (2022). Learning coefficient heterogeneity over networks: A distributed spanning-tree-based Fused-Lasso regression. *Journal of the American Statistical Association*, 0(0):1–13.
- Zhang, Z. and Wang, L. (2023). A simulation framework for reciprocal recurrent selection-based hybrid breeding under transparent and opaque simulators. *Frontiers in Plant Science*, 14:1174168.

Table 1: Average ARI and Average \hat{K} over 100 simulations under spatial grid lattice in Figure 2a. Standard deviation values are in parentheses.

method	ARI	\hat{K}
tree	0.569(0.052)	8.750(1.635)
adaptive	0.994(0.064)	2.010(0.100)
NPFSS	0.517(0.261)	1.840(0.443)
PFSS	0.019(0.109)	1.030(0.171)
DFSS	0.003(0.028)	1.020(0.141)
URBFSS	0.192(0.281)	1.370(0.485)
PSS	0.669(0.023)	2.000(0.000)
PPSS	0.669(0.023)	2.000(0.000)

Table 2: Average ARI and Average \hat{K} over 100 simulations under spatial random locations in Figure 2b. Standard deviation values are in parentheses.

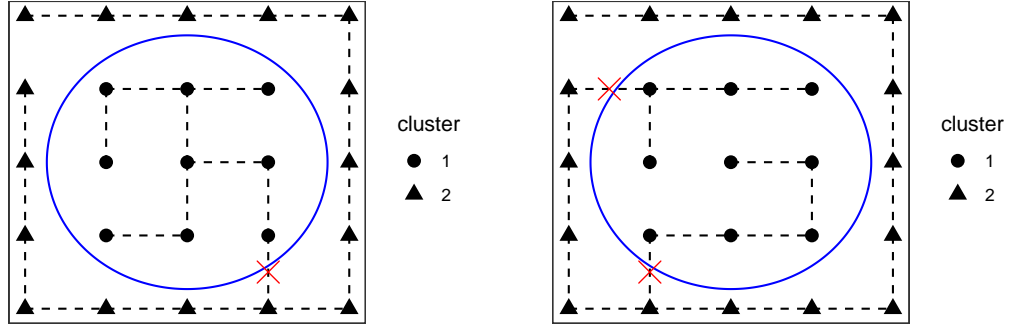
method	ARI	\hat{K}
tree	0.179(0.011)	9.680(0.737)
adaptive	1.000(0.000)	2.000(0.000)
NPFSS	0.800(0.123)	1.980(0.141)
PFSS	0.143(0.307)	1.200(0.402)
DFSS	0.003(0.030)	1.010(0.100)
URBFSS	0.079(0.175)	1.260(0.441)
PSS	0.516(0.055)	2.000(0.000)
PPSS	0.516(0.055)	2.000(0.000)

Table 3: Summary of results over 100 simulations under spatial grid lattice in Figure 3a

	algorithm	ARI	\hat{K}	F1	\hat{J}
Setting 1	tree	0.597(0.025)	16.680(1.399)	1.000(0.002)	2.010(0.100)
	adaptive	0.997(0.010)	5.020(0.141)	1.000(0.000)	2.000(0.000)
Setting 2	tree	0.576(0.022)	14.630(0.861)	1.000(0.002)	2.010(0.100)
	adaptive	0.961(0.048)	5.080(0.307)	1.000(0.000)	2.000(0.000)

Table 4: Summary of results over 100 simulations under spatial random locations in Figure 3b

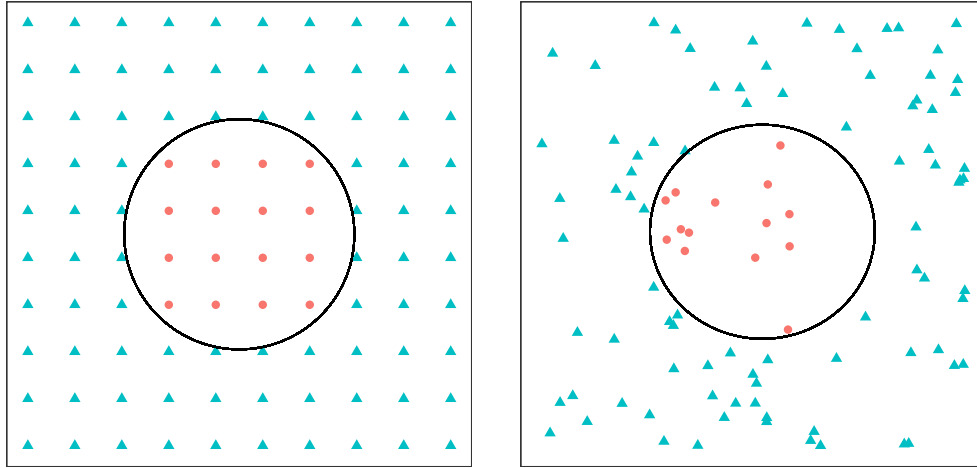
	algorithm	ARI	\hat{K}	F1	\hat{J}
Setting 1	tree	0.763(0.004)	13.090(1.016)	1.000(0.000)	2.000(0.000)
	adaptive	0.999(0.004)	5.010(0.100)	1.000(0.000)	2.000(0.000)
Setting 2	tree	0.763(0.009)	12.030(0.223)	1.000(0.000)	2.000(0.000)
	adaptive	0.986(0.016)	5.000(0.000)	1.000(0.000)	2.000(0.000)



(a) An example of a spanning tree with one edge between two clusters.

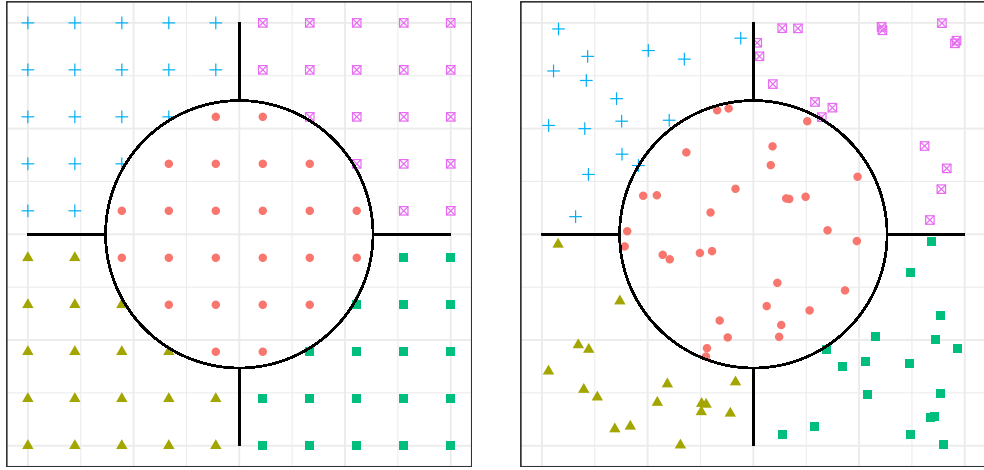
(b) An example of a spanning tree with two edges between two clusters.

Figure 1: Two spanning trees with 25 nodes. Different shapes represent two different clusters. Dashed lines represent edges connecting two nodes.



(a) Cluster structure for a 10×10 grid lattice (b) Cluster structure for 100 random locations.

Figure 2: True cluster structures for simulated data. The color and shape show the underlying cluster structure. The solid lines separate the 2 clusters.



(a) Cluster structure for a 10×10 grid lattice (b) Cluster structure for 100 random locations.

Figure 3: True cluster structures for simulated data. The color and shape show the underlying cluster structure. The solid lines separate the 5 clusters.

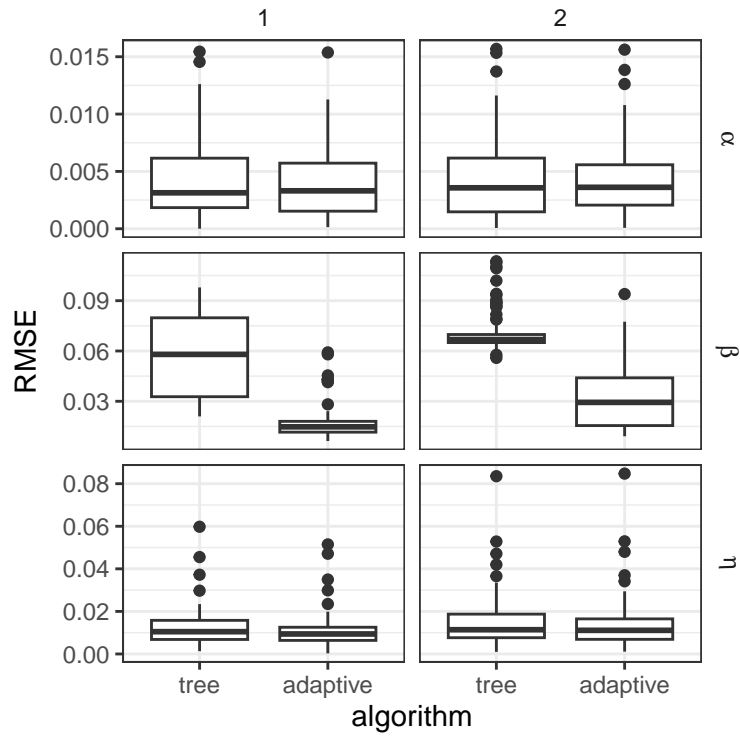


Figure 4: RMSE of different parameters under two parameter settings for spatial lattice grid. The left three figures are for α , β and η under Setting 1. The right three figures are for α , β and η under Setting 2.

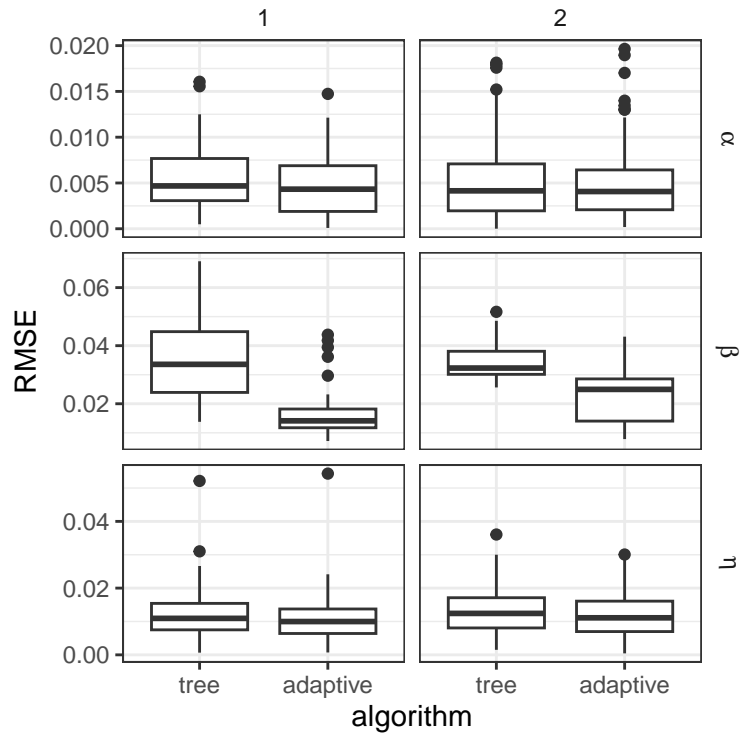


Figure 5: RMSE of different parameters under two parameter settings for spatial random locations. The left three figures are for α , β and η under Setting 1. The right three figures are for α , β and η under Setting 2.

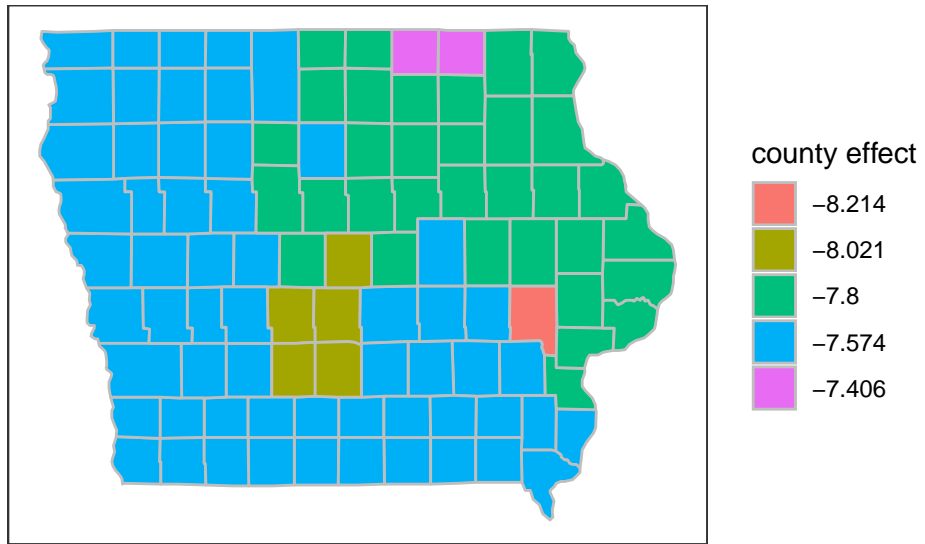


Figure 6: Estimated cluster structure of county effect